https://doi.org/10.5194/egusphere-2025-1463
Preprint. Discussion started: 28 May 2025

Diurnal variability and controlling mechanisms of marine aerosol distributions over the South China Sea: Insights from shipborne observations

Zhi Qiao[1,2,3], Shengcheng Cui[1,3,4,*], Huiqiang Xu[1,2,3], Xiaoqing Wu[1,3,4], Xiaodan Liu[1,2,3], Zihan Zhang[1,4], Mengying Zhai[1,2,3], Yue Pan[5], Tao Luo[1,4], Xuebin Li[1,4]

[1]Key Laboratory of Atmospheric Optics, Anhui Institute of Optics and Fine Mechanics, HFIPS, Chinese Academy of Sciences, Hefei 230031, China
[2]Science Island Branch of Graduate School, University of Science and Technology of China, Hefei 230026, China
[3]Nanhu Laser Laboratory, National University of Defense Technology, Changsha 410073, China
[4]Advanced Laser Technology Laboratory of Anhui Province, Hefei 230037, China
[5] School of Electronic Engineering, Chaohu University, Chaohu, 238024, China

Correspondence to: Shengcheng Cui(csc@aiofm.ac.cn)

Abstract. Marine aerosols critically influence Earth's radiation budget and climate dynamics through their spatial distributions and components due to their generation and transport processes. However, in-situ observational datasets remain limited, particularly in the South China Sea (SCS). Based on our comprehensive shipborne measurements, this study presents a quantitative analysis of marine aerosol distributions and compositional variations between the offshore and pelagic environments over the SCS. Our data demonstrate a 120% elevation in offshore aerosol number concentrations (NCs, 0.5-10 μm) relative to pelagic baselines, featuring 120% higher accumulation-mode particles (0.5-2 μm) and 70% higher coarse-mode particles (2-10 μm), quantitatively confirming continental transport affects offshore aerosol signatures. In contrast, in the pelagic areas, marine aerosols are virtually unaffected by continental transport and distinctly represent characteristics of the local generation. Meteorological analyses identified wind speed (WS) and sea surface temperature (SST) as primary regulators of NC. However, observed NC variations at fixed WS and SST values suggest additional controlling factors. We demonstrate that sea-air temperature differences (SST-T_{2m}) exhibit a stronger correlation ($r = -0.82$, $p<0.01$) with NC than the other meteorological parameters, where increased SST-T_{2m} corresponded to decreased marine aerosol production. This temperature gradient effect drives pronounced diurnal NC variations, with maximum differences of 35% observed between daytime, nighttime, and transition periods. These results prove the key explanations for the variations of spatial and diurnal distributions of marine aerosols to understand marine aerosol generation and transport better.

https://doi.org/10.5194/egusphere-2025-1463
Preprint. Discussion started: 28 May 2025

Graphical Abstract

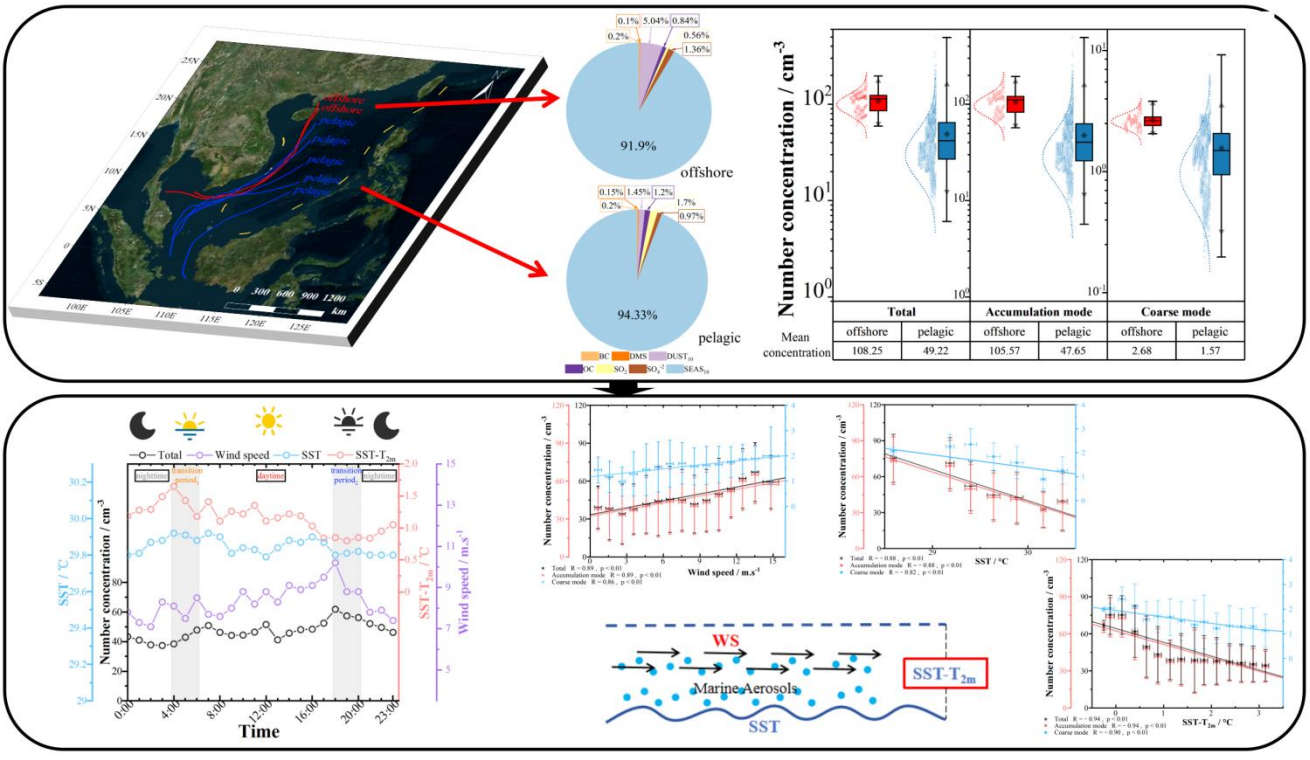

30 Keywords: Shipborne observation; marine aerosol distributions; aerosol generation and transport; sea-air temperature differences; the South China Sea

1. Introduction

Atmospheric aerosols constitute one of the most significant uncertainties in climate system projections, both historically and prognostically (Andreae & Rosenfeld, 2008; Bauer et al., 2020; Bzdek et al., 2020). As the ocean covers more than two-
35 thirds of Earth ' s surface, marine aerosols originating from sea surface emissions and atmospheric gas-to-particle conversion processes represent the dominant natural aerosol source globally (Korhonen et al., 2008; Nguyen et al., 2017; Textor et al., 2006). These aerosols are conventionally categorized as either anthropogenic or natural, with the latter primarily comprising sea salt particles and sea spray aerosols (Duce et al., 1965; Sander et al., 2003; Troitskaya et al., 2018). Through their radiation interactions, marine aerosols significantly influence both direct and indirect components of Earth's
40 energy budget (Decesari et al., 2011; Myhre et al., 2004; Woods et al., 2010). Their climatic impacts extend to modifying marine cloud microphysical properties (Feingold et al., 1999; Levin et al., 2005), regulating precipitation patterns (Woodcock, 1952, 1953) and driving surface ocean geochemical cycles (Alexander et al., 2005; Eriksson, 1960; Lawler et al., 2011; Long et al., 2014). Given these multifaceted roles in atmospheric processes, contemporary research

https://doi.org/10.5194/egusphere-2025-1463
Preprint. Discussion started: 28 May 2025

increasingly recognizes marine aerosols as critical regulators of the global climate system (Li et al., 2022; Meinrat & Paul, 1997).

Due to their non-negligible influence on both radiation budget and climate change, more and more research on marine aerosols has been conducted for forty years. Hoppel (1979, 1985) studied the aerosol NC and the particle size distribution on the east coast of the United States, and the significant changes in the particle size distribution can be associated with the changes in meteorological parameters and oceanic air mass. In addition, Prospero (1979) comprehensively reported the mineral and sea salt aerosol concentrations in several marine areas and found that the aerosol mass concentrations from one marine area to the other were relatively different, ranging from 3.34 to 8.71 μg m^{-3}. In the Arctic, Leck (1996) reported that the submicrometer aerosol (Dp ≤ 1000 nm) mass concentrations during the International Arctic Ocean Expedition (IAOE-91) cruise; for instance, the average mass concentration was 0.76 μg m^{-3} over the ocean. In terms of the Antarctic, Savoie (1993) reported the submicrometer aerosol (Dp ≤ 1000 nm) concentrations, and the mean concentrations were 3.15 μg m^{-3} at Marsh. Subsequently, Sakerin (2015) measured the marine aerosol (0.3 μm ≤ Dp ≤ 10 μm), and he found that the average mass concentration was 875 ng m^{-3} at the Chukchi and East Siberian seas. In the Indian Ocean, Pant (2009) observed that the average micrometer aerosols (0.5 μm ≤ Dp ≤ 10 μm) mass concentrations were 8.89 μg m^{-3}. For the China waters, Kim (2009) found that the average submicrometer aerosol particle (10 nm ≤ Dp ≤ 300 nm) concentrations were 4335 ± 2736 cm^{-3} over the East China Sea and 5972 ± 2736 cm^{-3} over the Yellow Sea. Han (2019) found that the daily average $PM_{2.5}$ (Dp ≤ 2500 nm) concentration was 140 ± 48.1 μg m^{-3} in the Bohai Sea. All in all, there were some discrepancies in the marine aerosol concentrations and size distributions between the different ocean areas; however, there were very few studies of the marine aerosol concentration and particle size distribution in the SCS, especially from 10° N-20° N (Kong et al., 2016; Ma et al., 2022; Su et al., 2022). Most measurement data were observed by the coastal monitoring station, and the shipboard observations are still very sparse in the SCS; moreover, the major measurement data are relatively outdated and need to be updated.

The aerosol generation and transport radically led to the differences in marine aerosol concentration and size distribution. Some studies revealed that aerosol components and particle size distribution were influenced by both the occurrence of weather events and the distance from the coast, and the aerosol transport was associated with the distances (Athanasopoulou et al., 2016; Chen et al., 2018; O'Dowd & De Leeuw, 2007; Sellegri et al., 2006). Furthermore, some key meteorological parameters of the air-sea interface could affect the aerosol generation and transport, such as SST, wind direction (WD) and speed (WS), relative humidity (RH), et al. (Carslaw et al., 2010; Hoppel, 1979). Tang (1997) found that the marine aerosol deliquescence (process of the water absorption till they were fully dissolved) and the efflorescence (process of drying until they returned to the crystalline structure) can be associated with the RH values. Therefore, the RH was one of the major factors affecting the marine aerosol concentration and particle size distribution by influencing the aerosol wet deposition and dispersion (Irshad et al., 2009; Wise et al., 2009; Zeng et al., 2013). Meanwhile, previous studies found that WS was the major driver of the production and transport of marine aerosols. Some subsequent studies attempted to link the NCs to the observed WS and created the generation functions simulating the concentrations by using the relationships (Andreas, 1998,

https://doi.org/10.5194/egusphere-2025-1463
Preprint. Discussion started: 28 May 2025

2002, 2010; Ovadnevaite et al., 2014; Smith et al., 1993). In addition, the SST dramatically influences the production of marine aerosols. They explained that the SST affected the sea surface water density, tension, and so on, all of which affected the bubble formation and bursting process and influenced the production of marine aerosols ultimately (Jaeglé et al., 2011; Mårtensson et al., 2003; Zábori et al., 2012a). As aforementioned, changes in the offshore distances and these meteorological parameters will influence marine aerosol NC and particle size distribution. However, previous studies indicated that SST-T_{2m} influences the air-sea interaction through air-sea heat exchanges and turbulent mixing; meanwhile, it can comprehensively reflect the characteristics of the ocean and atmosphere near the sea surface (Jing et al., 2019; Ma et al., 2016; O'Neill et al., 2010). Hence, SST-T_{2m} might affect marine aerosol generation and transport, but the exact effects of SST-T_{2m} on marine aerosols need further investigation. For better quantifying and understanding the effect of these factors on marine aerosols, more thorough information about the variations of marine aerosol and these factors, especially for SST-T_{2m}, was needed in the SCS.

In summary, most observation data of the marine aerosols and the meteorological parameters were relatively outdated in the SCS; the subsequent updates simultaneously were lacking. Meanwhile, there was a probable relationship between meteorological element change and marine aerosol. Notably, meteorological parameters exhibited significant variations within and between different oceanic regions in terms of the primary factors influencing aerosol generation and transport, implying that the responses of marine aerosol distributions to changes in meteorological parameters could also vary among these areas. Moreover, there was a lack of studies on the scale of the diurnal changes in marine aerosol distributions, and an urgent need for their specific connection to meteorological parameters and distance from the coast to understand aerosol generation and transport better. To address these, we acquired and updated the observations of marine aerosol and meteorological parameters, then quantitatively compared the marine aerosol distributions and components in the offshore and pelagic environments over the SCS, as well as the influence of aerosol transport on marine aerosol. Afterward, the temporal variations of the shipborne observed data were investigated in detail; meanwhile, the discrepancies in the distribution of the marine aerosol in the diurnal variations, especially the diurnal transition, were further analyzed. According to these analyses, the specific relationships between the different meteorological parameters and marine aerosols were examined respectively; finally, the overall results of marine aerosol particle size distributions and NCs in the SCS and the possible influence factors were given.

2. Cruise observation and data analysis

2.1. Cruise details

In May and June 2023, the South China Sea Institute of Oceanology, Chinese Academy of Sciences carried out a science cruise program in the SCS onboard *Yuezhanyuke NO. 6*. This study analyzes the aerosol-meteorology (AM) measurements along the section from the latitude 21°02′ N to 8°5′ N and the longitude 110°33′ E to 115°25′ E. All the AM data were collected from 21 May to 15 June 2023.

https://doi.org/10.5194/egusphere-2025-1463
Preprint. Discussion started: 28 May 2025

2.2. Instrument setup

2.2.1. Aerosol sampling instrument

The NCs of aerosol particles were measured with the Model 3321 Aerodynamic Particle Size (APS) spectrometer (TSI Incorporated, USA), which has 52 size channels in the 0.5 to 20 μm range. This Model 3321 APS spectrometer employs relative light-scattering intensity along with sophisticated time-of-flight techniques; the two complementary techniques can measure the information of each aerosol particle to obtain the aerosol concentrations and distributions. The accuracy of the aerosol data for particle diameters between 0.5 μm and 10 μm, as measured by the Model 3321 APS spectrometer, had been fully validated in previous studies (Pagels et al., 2005; Peters et al., 2003; Peters, 2006). Meanwhile, we used the Particle Loss Calculator (PLC) to calculate the particle losses for the Model 3321 APS spectrometer in this cruise (Fig. 1) (Von Der Weiden et al., 2009). Fig. 1 showed that the particle losses were small in the size range from 0.5 μm and 10 μm. Thereby, aerosol data within the size range of 0.5 to 10 μm were selected for future analysis in this study.

The Model 3321 APS spectrometer was loaded in the captain's cabin and coupled with a 10-cm long tube and a 1.8 cm internal diameter, as shown in Fig. 2a. The tube was fixed in an exterior wall of the captain's cabin at 30° to the horizontal and faced the direction of the sea surface. Meanwhile, the tube's inlet was approximately 7 m above the mean water level, and this location was thought to be less affected by human factors and the bow splashing. The flow rate was 1.0 liter per minute, and the sample length was 15 seconds. The atmospheric aerosol data resolution was set to 5 min in this SCS cruise observation. The detailed definition and calculation formula for aerosol number concentration were shown below.

$$n = \frac{c}{lQ}\frac{\Phi}{\eta}, \qquad (1)$$

where n is the number concentration per channel, c is the particle counts per channel, l is the total sample time, Q is the sample flow rate, Φ is the sample dilution factor, and η is the sample efficiency factor per channel.

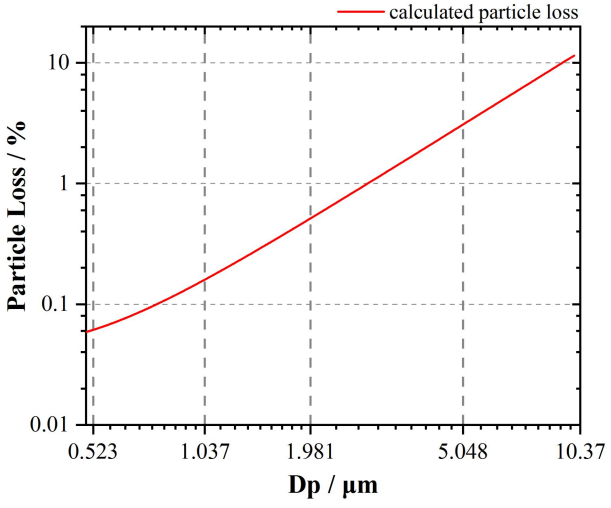

https://doi.org/10.5194/egusphere-2025-1463
Preprint. Discussion started: 28 May 2025

Fig. 1 The calculated particle losses for the Model 3321 APS spectrometer in this cruise.

2.2.2. Meteorological instruments

The automatic meteorological observation system (AMOS), including the Vaisala WXT530 weather station, the Campbell CSTA3B sonic anemometer, and the Belfort Model 6400 visibility sensor, was installed on the top deck to continuously observe the meteorological observation data. The height of the AMOS above the mean water level was approximately 10 m, as shown in Fig. 2b. The Vaisala WXT530 measured the atmospheric parameters such as air temperature (T_{OBS}), RH and rainfall intensity with a temporal resolution of 1 s. The two-dimensional wind field (i.e., the horizontal components u_x and u_y) was measured by the Campbell CSAT3B, and the temporal resolution was 0.05 s. To support the ancillary research, the Belfort Model 6400 observed the atmospheric visibility (VIS) with a temporal resolution of 1 s. More detailed descriptions of the AMOS were listed in Table 1.

Table 1

Configurations and specifications of AMOS

WXT530		CSTA3B		Model 6400	
Performance index	Description	Performance index	Description	Performance index	Description
Observation Range (T_{OBS})	-52 ~ +60 ℃	Observation Range (WS)	0 ~ 60 m s^{-1}	Observation Range (VIS)	0 ~ 50 km
Resolution (T_{OBS})	0.1 ℃	Resolution (WS)	0.1 m s^{-1}	Resolution (VIS)	0.1 km
Accuracy (T_{OBS})	±0.3 ℃	Accuracy (WS)	±0.3 m s^{-1}	Accuracy (VIS)	±1 km
Observation Range (RH)	0 ~ 100 %	Observation Range (WD)	0 ~ 360°		
Resolution (RH)	0.1 %	Resolution (WD)	1°		
Accuracy (RH)	±3 %	Accuracy (WD)	±3°		
Observation Range (Rain)	0 ~ 200 mm h^{-1}				
Resolution (Rain)	0.1 mm h^{-1}				
Accuracy (Rain)	±0.5 mm h^{-1}				

https://doi.org/10.5194/egusphere-2025-1463
Preprint. Discussion started: 28 May 2025

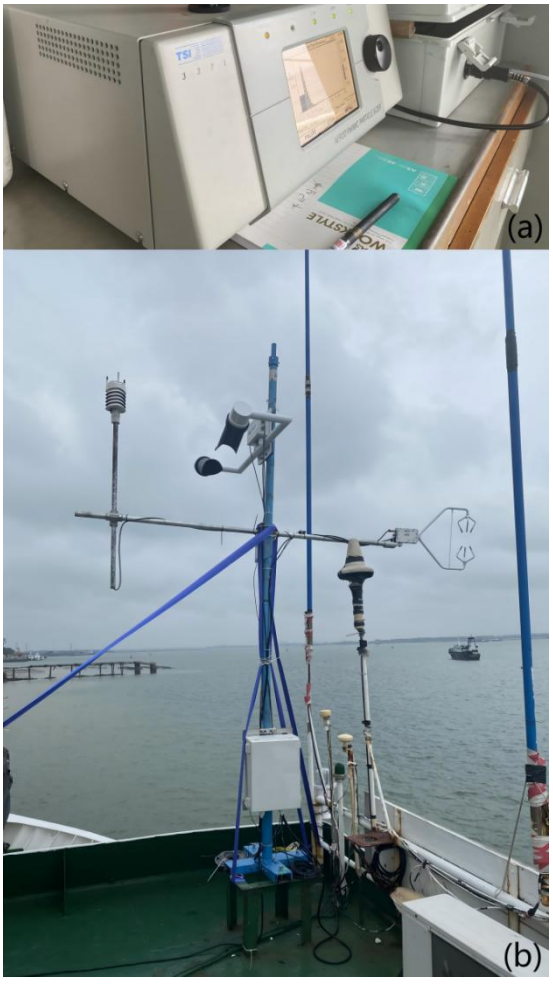

Fig. 2 The total view of (a) the Model 3321 APS spectrometer and (b) the automatic meteorological observation system.

2.3. Auxiliary data

2.3.1. Reanalysis data

In this study, the 10-m wind speed (WS_{10}), direction (WD_{10}), and friction velocity (U_{zust}) were obtained from the ERA5 hourly dataset with a spatial resolution of 0.25° × 0.25°. The ERA5 hourly dataset used in this study was provided by the European Centre for Medium-Range Weather Forecasts (ECMWF) (Hersbach et al., 2023). In order to determine the values of SST-T_{2m}, we needed to know the temperature at 2 m (T_{2m}) and SST. Meanwhile, the Merra-2 SST reanalyzed data was in excellent agreement with the observed SST data ($r > 0.9$) (Jiang et al., 2021). We selected the SST and T_{2m} data from the Merra-2 meteorological dataset in this context.

For the atmospheric aerosol component data, the NASA Goddard Space Flight Center Merra-2 aerosol dataset was used in this study due to its good performance over Europe and China (Provençal et al., 2017a & 2017b). The Merra-2 aerosol

https://doi.org/10.5194/egusphere-2025-1463
Preprint. Discussion started: 28 May 2025

dataset consisted of the assimilated aerosol diagnostics data, such as the surface mass concentrations of aerosol components (i.e., sea salt (SEAS), dust, black carbon (BC), sulfate, and organic carbon (OC)) with a spatial resolution of 0.5° × 0.625° and a temporal resolution of 1 hour (Global Modeling and Assimilation Office (GMAO), 2015). We used the above aerosol component data to discuss the discrepancy in aerosol distribution over the SCS.

160

2.3.2. Back trajectory analysis

The Hybrid Single-Particle Lagrangian Integrated Trajectory (HYSPLIT) transport and dispersion model (http://www.arl.noaa.gov/ready/hysplit4.html), developed by the National Oceanic and Atmospheric Administration Air Resources Laboratory (NOAA ARL), was employed to analyze the air mass backward trajectory. The meteorological data
165 for the backward trajectories was obtained from the Global Data Assimilation System (GDAS) archive dataset (http://ready.arl.noaa.gov/gdasl.php). The backward trajectories were calculated for 72 h. Meanwhile, the trajectories were calculated at an altitude of 50 m, and the top of the HYSPLIT model was set to 5,000 m to clarify the influence of the source region on the marine aerosols.

2.4. Contaminated data screening

170 To observe actual aerosol loadings in the typical marine environment, excluding aerosol observation data contaminated by ship emissions during the cruise (including the periods subject to the offshore and the pelagic) is necessary. To achieve this, we performed quality control during the aerosol observation data collection with the accompanied WS, WD, rainfall intensity, and total aerosol number concentration data as follows:

i) *Data screening with wind observations*. The north arrow of the Vaisala WXT530 was oriented perpendicular to the ship's
175 longitudinal axis, pointing east relative to the vessel's heading. The observed WD thus represented the relative angle between the wind direction and the ship's course. When the ship was sailing, the WD sampled ranged from 225° to 315°. We excluded these sampled data because the aerosol observations were directly affected by the ship emissions. As depicted in Fig. 3a, one can easily find a sharp decrease and increase in the observed aerosol size distributions on 25 May. The underlying cause of the abnormal changes in aerosol size distribution could be the removal of the coarse aerosol mode
180 by the rainfall, as depicted in Fig. 3b. However, this "jump" was located at 7:00 a.m. (circled in black in Fig. 3a) while the rainfall occurred at 8:00 a.m. and lasted for about 6 hours, so it is not the rainfall that influences the data jump in aerosol size distribution. With the help of the WD sequence data shown in Fig. 3b (circled in red), we found that the jump in the WD curve was also located at 7:20 a.m. and thus identified the accurate cause of the aerosol data jump; it is the wind direction rather than the rainfall that led to the anomaly in aerosol size distributions.

185 ii) *Further data screening with unreasonable NCs*. The new aerosol generation events often accompanied the increased nucleation events. The previous studies indicated that the nucleation events observed in marine environments were characterized by different shapes, in the aerosol size distributions versus time series plots. However, all the nucleation events

https://doi.org/10.5194/egusphere-2025-1463
Preprint. Discussion started: 28 May 2025

last at least several hours at the sea surface (Kuang et al., 2009; Ehn et al., 2010), due to the persistent growth of these aerosol particles. So, we excluded the sharp decrease and increase in NCs data in the short term without changes in the meteorological parameters and influences of continental transport, and all the excluded data had NCs that were one order of magnitude higher or lower than the average NC at that time. So that further screen out the possible influences produced by the ship emissions.

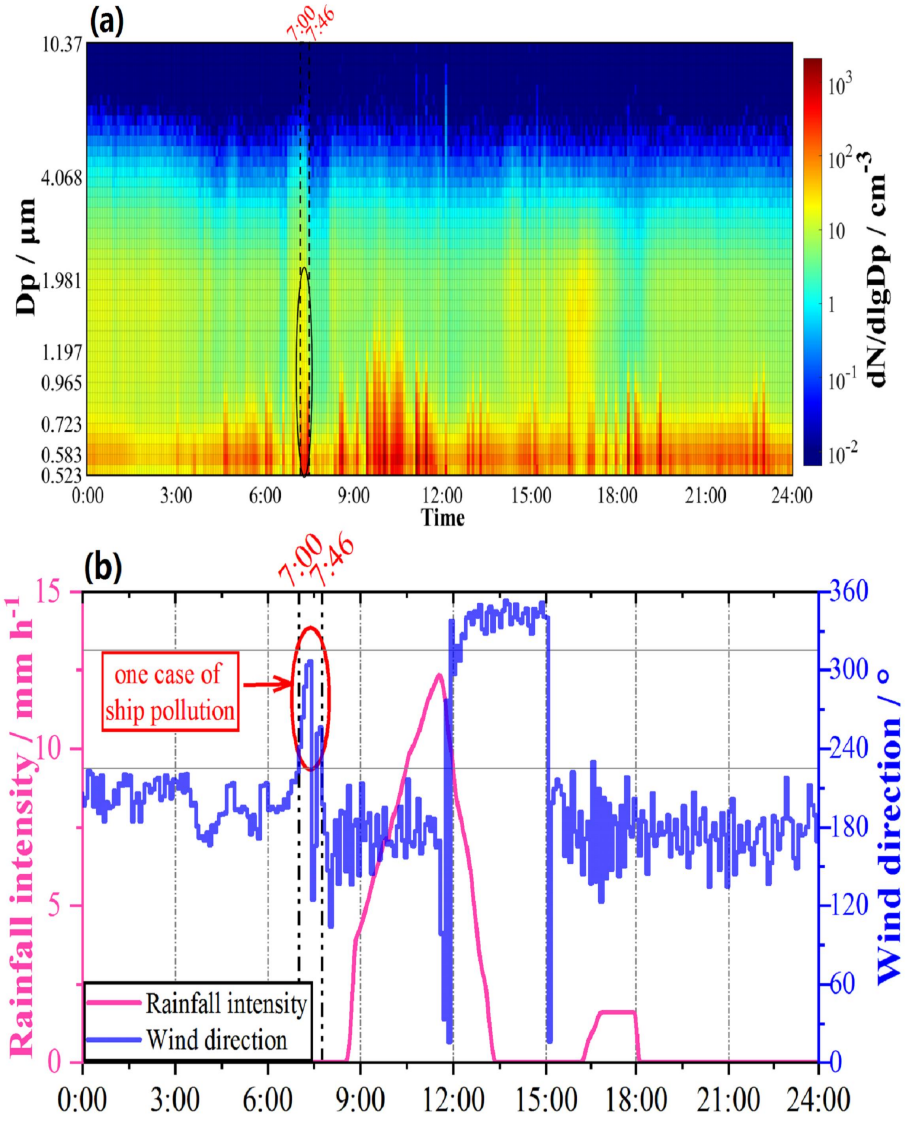

Fig. 3 The time series of the observations on 25 May 2023. The black circle represented one case of ship pollution. (a) Trends of the aerosol size distributions. (b) Trends of the rainfall intensity and the WD.

https://doi.org/10.5194/egusphere-2025-1463
Preprint. Discussion started: 28 May 2025

3. Results and discussion

3.1. Temporal distributions of the observations

Fig. 4 showed the time series of the marine aerosol distributions and the meteorological parameters during the observation of the shipboard in the SCS. Due to the pump of the Model 3321 APS spectrometer failing to work from 4 June to 15 June 2023 during the cruise period, the flow rate could not reach the minimum standard. Thus, we only analyzed variations of the observation data from 21 May to 3 June 2023. Fig. 4 a-b presented the trends of the aerosol size distribution and the comparison of the accumulation and coarse mode particle NCs. During the shipboard observation period, the average total marine aerosol NC was 54.01 ± 35.37 cm^{-3}, the NC of aerosol accumulation mode was 52.35 ± 34.96 cm^{-3}, and the NC of aerosol coarse mode was 1.66 ± 0.83 cm^{-3}. We found that the marine aerosol NC changed drastically with the temporal differences during the shipboard observation period. Meanwhile, the published observation data of the marine aerosol NC relevant to this study were shown in Table 2. Due to the constraints of the geographical location and the data acquisition, we listed some relevant shipboard observation data. The shipboard observation data recorded and showed the overall average values and standard deviations of marine aerosol NCs under different temporal and geographical conditions, which were used to compare with the marine aerosol NCs observed.

In this study, the observed NC of accumulation mode was more consistent with the 2005 SCS observation (Lin et al., 2007) but lower than the observation in the East China Sea (Lin et al., 2007; Ma et al., 2022). This suggested that the NC of aerosol accumulation mode in the East China Sea might affected by the higher frequency of the new marine aerosol particle formation and the more frequent continental source transport at the westerlies. Hence, the aerosol accumulation mode was significantly lower in the SCS. Meanwhile, the total marine aerosol NC observed in this study contained the aerosol coarse mode (2 μm ≤ Dp ≤ 10 μm) and the part of aerosol accumulation mode (500 nm ≤ Dp ≤ 2000 nm), and the NC was slightly lower than the marine aerosol NC in the Atlantic by Flores et al. (2020). Regarding the marine aerosol NCs in the same region, the observations of Cai et al. (2020) and Kong et al. (2016) were significantly higher than the observations in this study. Although the differences in the observation seasons, the study region, and the particle size might influenced the average NC observations, it can still show that the marine aerosol was significantly affected by the continental transport and the anthropogenic activity in the offshore areas according to the latitude and longitude.

Wet deposition through scavenging by rainfall process is a critical sink for aerosols (Atlas & Giam, 1998; Radke et al., 1980). However, some studies found that the aerosols might be generated on the porous surface when impinged by liquid droplets (Bird et al., 2010; Joung & Buie, 2015; Zhou et al., 2020). Thereby accounting for the observation environment and rainfall intensity, short-duration heavy rainfall resulted in numerous raindrops impacting the ocean and ship surfaces, generating aerosol particles. Subsequently, the monitoring instrument captured some of these aerosol particles, ultimately contributing to the increased aerosol particle concentration observed in Fig. 4 (the blue-shaded regions). In addition to the elevated concentrations of marine aerosols resulting from these rain events, the aerosol NC spectrum distributions shown in Fig. 4a demonstrate continuous marine aerosol number concentration distributions in the size ranges of 523 to 583 nm, 1715 to 1981

https://doi.org/10.5194/egusphere-2025-1463
Preprint. Discussion started: 28 May 2025

nm, and 4068 nm during the cruise period, which indicated the background characteristics of marine aerosol particle distributions in the marine environment. Meanwhile, during the cruise period, comparisons of the time series of the NCs between the two aerosol particle modes were made, as shown in Fig. 4b. The temporal trend of the NC of accumulation mode was approximately consistent with the coarse mode. The correlation coefficient between the two aerosol particle modes was R = 0.71. However, there were some discrepancies in the NC of the different particle sizes in aerosols caused by the different marine aerosol sources, and we found that the temporal trend of the accumulation mode was more variable than the coarse mode. Therefore, the accumulation mode was more obviously influenced by changes in the marine environment. For the meteorological parameters, the ship remained in the northeast trade winds during the whole cruise period; therefore, this mainly led to the South-Westerly and Southerly winds, as shown in Fig. 4c. Fig. 4d represented the air temperature and the water temperature. The observed air temperature was in excellent agreement with the reanalyzed air temperature from Merra-2, whereas the average T_{2m} and SST over the whole observation period were closer to 29.0 ℃ and 29.7 ℃. The RH had an obvious negative correlation with the visibility (R = -0.74), and the average RH and VIS were equal to 83.0 % and 45.1 km. Meanwhile, due to wind being the major driver of the production and transport of marine aerosols, we attempted to explain marine aerosol NCs of the accumulation mode and the coarse mode as the functions of the WS and WD (Fig. 5a, b). The RH and the rainfall intensity observations were used to aid analysis (Fig. 5c, d). High NCs (≥ 150 cm^{-3}) were observed almost entirely in which the WD were between NW and N that were caused by the high RH accompanied by the rainfall events, and the distributions of NCs were uniform when the wind was blowing in the other directions. Fig. 6 showed the variations of the NCs of two aerosol particle modes with the WS, and the observation data were binned to the WS intervals equal to 3 m s^{-1}. The variations in the NCs with the WS observed in this study were in accordance with the previous study (Bruch et al., 2023). For example, the NCs changed little in the region of 0-6 m s^{-1} WS because the WS was low for activation of the spume droplets and the marine aerosol generations. The NCs obviously increased with the increase in WS from 6 m s^{-1} to 15 m s^{-1}; however, the increase slowed down when the WS exceeded 13 m s^{-1}. The previous study proposed that the phenomenon was linked to scavenging marine aerosols through aerosol collision by the larger water drops at high WS (Pant et al., 2009).

Table 2

Summary of the available study results on the observed marine aerosol NC (cm^{-3})

Region	Time	Latitude	Longitude	Parameter	Value	Parameter	Value	Reference
South China Sea	2023.05 - 2023.06	21°N - 8°N	115°E -110°E	Accumulation mode	52.4 ± 35.0	$n_{500\text{-}10000}$	54.0 ± 35.3	This Study
South China Sea	2018	23°N -19°N	118°E -108°E	$n_{10\text{-}400}$	3400	$n_{400\text{-}32000}$	61	Cai et al., 2020
South China Sea	2012.09 - 2012.10	21°N -20°N	118°E -113°E	$n_{120\text{-}10000}$	175			Kong et al., 2016

https://doi.org/10.5194/egusphere-2025-1463
Preprint. Discussion started: 28 May 2025

South China Sea	2005.05	20°N -18°N	118°E -113°E	Accumulation mode	50.3 ± 19.5			Lin et al., 2007
East China Sea	2005.05	30°N -26°N	122°E -117°E	Accumulation mode	109.2 ± 51.8			Lin et al., 2007
East China Sea	2018-2019	28°N -20°N	130°E -120°E	$n_{250\text{-}2500}$	57.4 ± 40.9	$n_{2500\text{-}10000}$	57.5 ± 41.3	Ma et al., 2022
Atlantic	2016	60°N -30°N	80°W - 0°	$n_{100\text{-}19800}$	83			Flores et al., 2020
North Atlantic	2015	50°N	4°W	$n_{1000\text{-}6000}$	24			Yang et al., 2019

Note. In the column of the "Parameter", "n" indicated the NC and the subscripts indicated the particle size (nm); in the column of the "Latitude", "N" represented north latitude. The results of this study and these references were the overall average aerosol NCs.

https://doi.org/10.5194/egusphere-2025-1463
Preprint. Discussion started: 28 May 2025

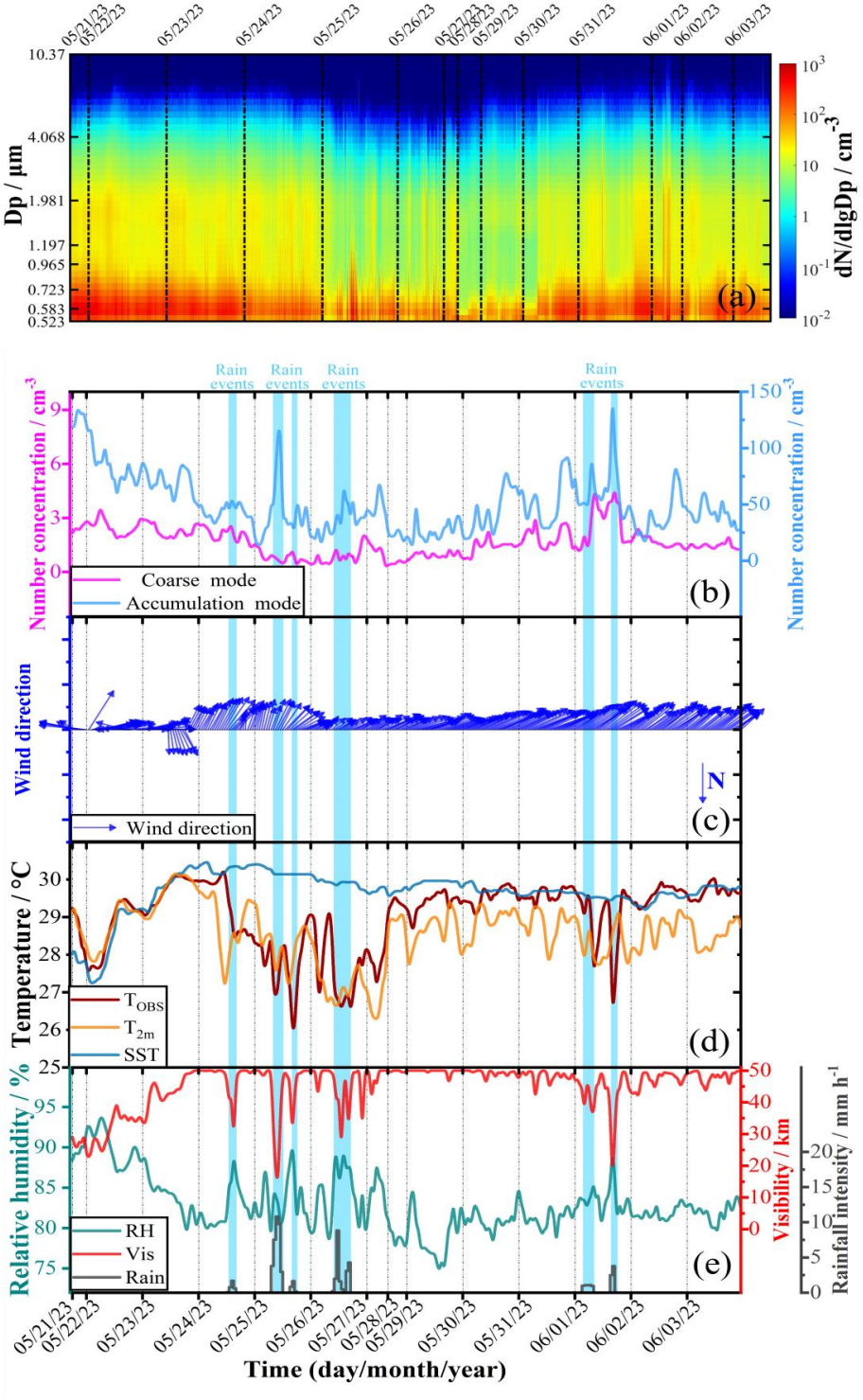

https://doi.org/10.5194/egusphere-2025-1463
Preprint. Discussion started: 28 May 2025

Fig. 4 The time series of the shipboard observations in the SCS from 21 May to 3 June 2023. The blue-shaded regions represented periods affected by rain events. (a) Trend of the aerosol size distributions. (b) Trends of NCs of the two aerosol particle modes (black solid line represented the NC of the coarse mode, and red solid line represented the NC of the accumulation mode). (c) Trend of the WD. (d) Trends of the T_{OBS} (dark orange solid line), T_{2m} (light orange solid line), and SST (blue solid line). (e) Trends in the RH (gray solid line), the VIS (red solid line), and the rainfall intensity (dark blue solid line).

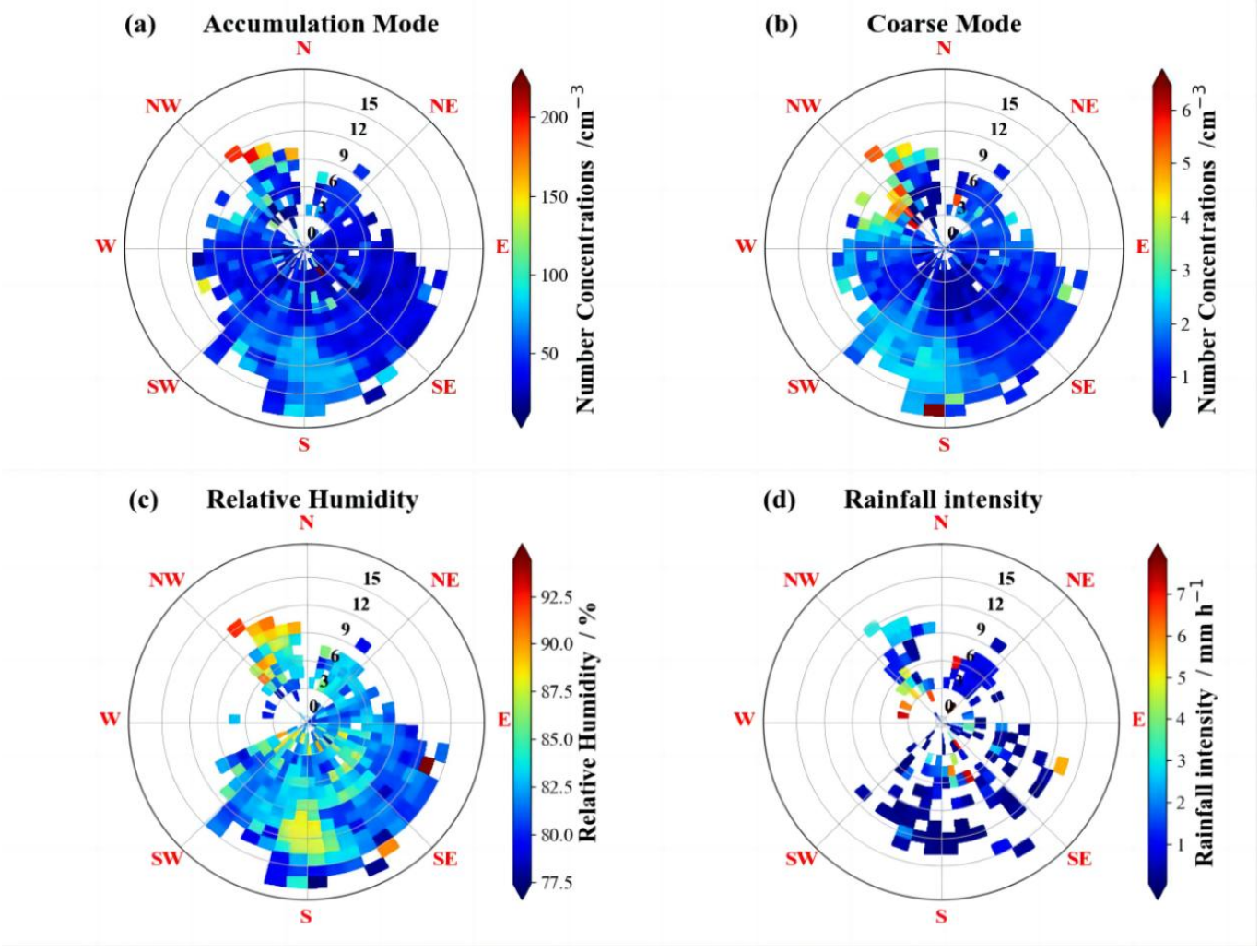

Fig. 5 (a) NC of the aerosol accumulation mode, (b) NC of the aerosol coarse mode, (c) RH, and (d) rainfall intensity as the functions of the WS and WD for the observations in the SCS.

https://doi.org/10.5194/egusphere-2025-1463
Preprint. Discussion started: 28 May 2025

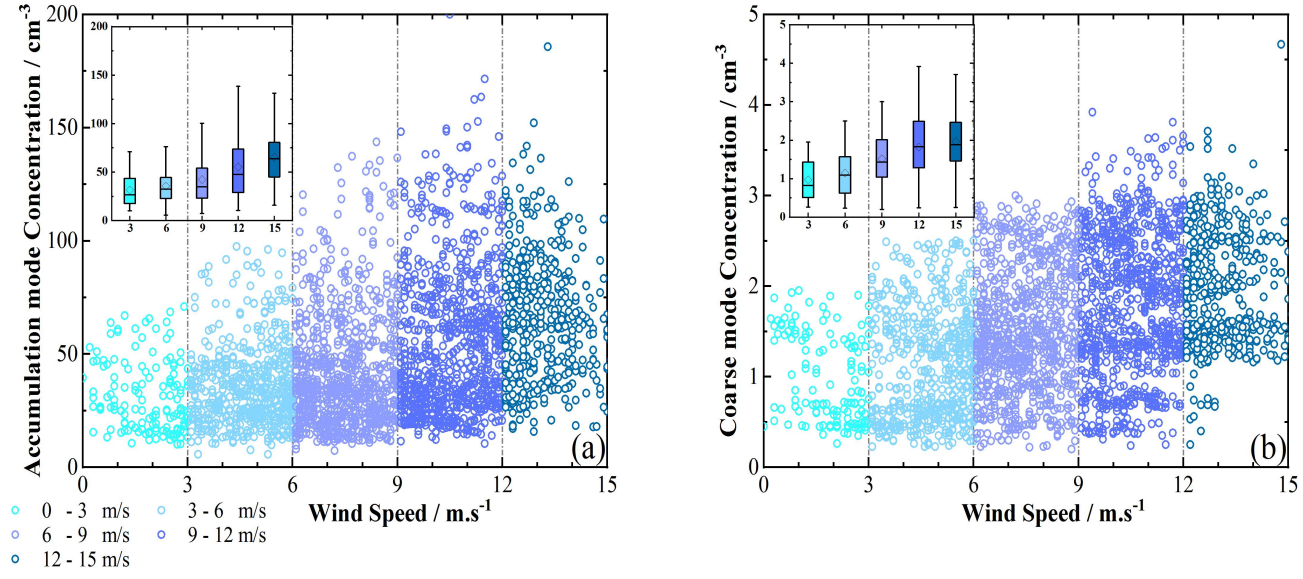

Fig. 6 The scatter plots of (a) NCs of the aerosol accumulation mode and WS, (b) NCs of the aerosol coarse mode and WS. The observation data were binned to the WS intervals equal to 3 m s^{-1}; the boxes represented the 25th to 75th percentile value, the black whisker represented the 1.5 inter-quartile range, the black diamond marker represented the mean value, and the black horizontal line represented the median value in the box plots.

3.2. Marine aerosol distributions in the different distance from the coast

This marine scientific research campaign started southward from the harbor of Zhanjiang (21°16′21.12″ N, 110°23′45.17″E) on 21 May and reached up to the southernmost (8°5′ N) point of this cruise on 3 June. In the different latitudes of the SCS, there were vastly different marine aerosol distribution characteristics, meteorological parameters, and marine aerosol transport sources. Therefore, we assessed the features of the marine aerosol distribution at various distances from the coast. We used the ArcGIS path distance method to calculate the distances from the coast and analyze the influences of distances on marine aerosols. In the equidistant projection, the ship positions were used as the input data, and the data of the coastline positions were used as the reference lines for the distance analyses. Considering the actual surface distance and horizontal and vertical factors, the shortest distance can be calculated from the ship to the coastline positions. Meanwhile, the distance from the coast of 50 km was taken as the boundary distance to distinguish the offshore and pelagic regions in this study. Hence, we can analyze the differences in aerosol transport and generation in the offshore and pelagic regions. Meanwhile, we removed the aerosol data, which was associated with greater than 1 mm h^{-1} rainfall intensity in the observation time, to eliminate the effects of the wet deposition on aerosol generation.

Fig. 7 showed the marine aerosol distribution characteristics with different modes in the SCS. From Fig. 7a, we can find that the NCs of different aerosol particle modes in the offshore areas showed significant differences from those in the pelagic areas. The average NC of the total marine aerosols in the offshore areas during the cruise period was 108.25 cm^{-3}, 2.2 times higher than the NC in the pelagic areas (49.22 cm^{-3}). Meanwhile, the NC of the accumulation mode in the offshore areas was

https://doi.org/10.5194/egusphere-2025-1463
Preprint. Discussion started: 28 May 2025

105.57 cm^{-3}, and it was 47.65 cm^{-3} in the pelagic areas. The average NC of the accumulation aerosol mode in the offshore areas was 1.2 times higher than that in the pelagic areas. However, the NC of the coarse mode comparison revealed that the result differed from the accumulation mode comparison, with little differences in the offshore and pelagic regions, where the NCs of the coarse mode in the offshore areas were 2.68 cm^{-3} and 1.57 cm^{-3} in the pelagic areas. Fig. 7b showed the number size distribution for marine aerosols of 0.5 to 10 μm diameters in the offshore and pelagic regions, where the $dN/dlgD_p$ represents the number size distribution. The comparisons in Fig. 7b showed that the number size distributions in the offshore and pelagic regions showed the bimodal distribution, and the peak values both occurred at 0.542 and 1.981 μm marine aerosol particle sizes. The marine aerosols were evenly distributed in the 0.835 to 1.981 μm particle size range. The marine aerosols decreased slowly with the increasing particle diameters below 1.114 μm due to the transport effect. The size distributions in the offshore areas were obviously higher than in the pelagic areas in the 0.5-5.0 μm particle size range. However, in the 5.0-10 μm particle size range, the number size distributions in the offshore areas were in excellent agreement with those in the pelagic areas. It was obvious from Fig. 7c that the NC was highly correlated with the distance from the coast, and the NC of the accumulation mode showed a significantly decreasing trend with the increasing distance from the coast (R = -0.87). We can find that R = -0.59 for the offshore distribution and R = -0.28 for the pelagic distribution, which showed that the correlation between distance from the coast and NC of accumulation mode was mainly reflected in the offshore areas and had almost no influence on the marine aerosol in the pelagic areas. The same was true for the coarse mode; the correlation between the coarse mode and the distance was -0.50 in the offshore areas and -0.33 in the pelagic areas. In other words, the aerosol distribution in the near-land and offshore regions was accompanied by the obvious aerosol transport phenomenon. After the ship entered the pelagic area, the influence of air mass transport almost disappeared. The marine aerosol NCs had been kept lower in the pelagicarea.

From Table 3, we can see that the meteorological element distributions in the offshore areas were significantly different from those in the pelagic areas. For example, the average WS in the offshore areas was 10.74 m s^{-1}, slightly higher than in the pelagic areas (8.64 m s^{-1}). Therefore, there was a higher generation of aerosols in the offshore areas. In addition to the WS influence, the frequency of southwest and west winds was high in the offshore environments. The distance from the coast ocean was short in the offshore region, which was accompanied by the aerosol transporting from Guangzhou and Hainan provinces, China (Fig. 8b). Fig. 8a showed the distributions of the backward trajectory air mass in the offshore and pelagic regions. The air masses passed over the mainland areas, which carried the continental aerosols and ultimately influenced the aerosol distributions in the offshore environments. However, on the one hand, the prevailing wind direction was primarily from the southwest (Fig. 3c) during the pelagic observation period, and the air masses did not directly pass over the mainland areas. On the other hand, the continental and anthropogenic aerosols, which were emitted from islands and countries surrounding the SCS, underwent atmospheric transport, transformation, and deposition processes. This results in gradual dilution and mixing with natural aerosols. Over time, the continental and anthropogenic aerosols transformed or integrated into the background aerosol, losing their original characteristics (Gathman, 1983; Nascimento et al., 2021; Solomon et al., 2011). Therefore, in the pelagic environments, the marine aerosol was not significantly affected by aerosol transport and

https://doi.org/10.5194/egusphere-2025-1463
Preprint. Discussion started: 28 May 2025

anthropogenic activity. There existed a significant difference in the distributions of marine aerosol components between the offshore and pelagic regions (Fig. 7d). The proportions of the dust ($DUST_{10}$; Dp ≤ 10 μm) and sulfate aerosols (SO_4^{2-}) in the offshore areas were higher than those in the pelagic areas, indicating that the continental aerosol significantly influenced the aerosol components in the offshore environments. Meanwhile, due to the higher frequency of marine biological activities in the pelagic environments, the proportions of the dimethyl sulfide (DMS), organic carbon (OC), and sulfur dioxide (SO_2) aerosols were 0.15 %, 1.2 %, and 1.7 % and higher than those in the offshore environments, which were 0.1 %, 0.84 %, and 0.56 %, respectively. The proportion of sea salt aerosol ($SEAS_{10}$; Dp ≤ 10 μm) in the pelagic areas was higher than that in the offshore areas (94.33 % and 91.9 %), reflecting higher marine aerosol production in the pelagic environments. To sum up, our results indicated that the distance from the coast had a great influence on marine aerosol generation and transport. It ultimately led to the obvious discrepancy between the size distributions of the marine aerosols in the offshore and pelagic regions.

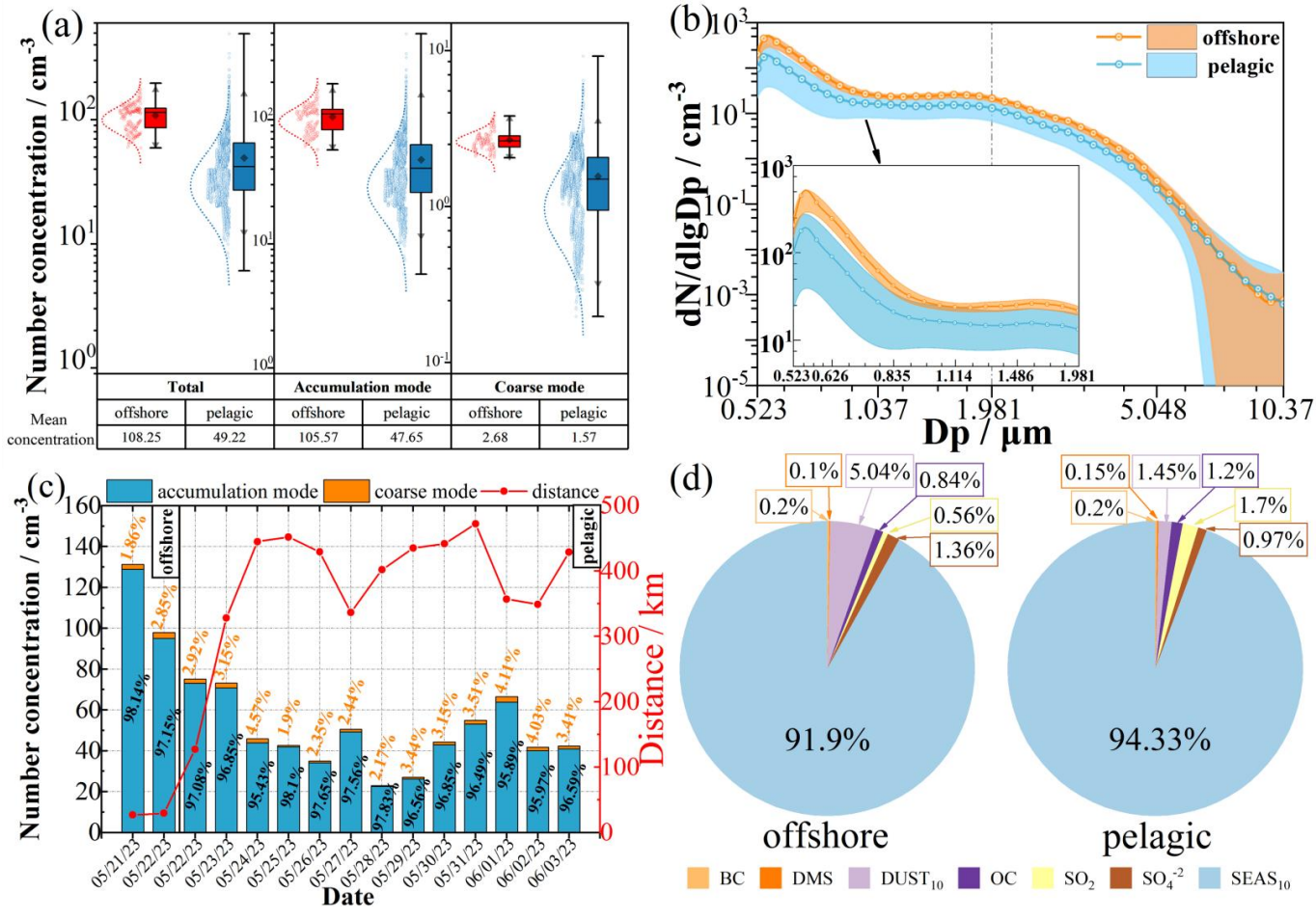

Fig. 7 Classification of the shipboard observation path in the SCS: (a) Accumulation and coarse mode particle sizes graded NCs in the offshore and pelagic regions. For the box plots, the boxes represented the 25th to 75th percentile value, the black whisker

https://doi.org/10.5194/egusphere-2025-1463
Preprint. Discussion started: 28 May 2025

represented the maximum and minimum range, the black triangle represented the 1.5 inter-quartile range, the black diamond marker represented the mean value, and the black horizontal line represented the median value. (b) The NCs of average size distributions (the solid lines and circles) and standard deviations (the shaded areas) for marine aerosols of 0.5 to 10 μm diameters in the offshore and pelagic regions. (c) The diurnal variations of the proportions and the NCs of two aerosol particle modes were shown with the distances from the coast. (d) The distributions of marine aerosol components in the offshore and pelagic regions. The pie charts showed the average aerosol composition based on the mass concentrations from the Merra-2 aerosol dataset during the whole cruise period.

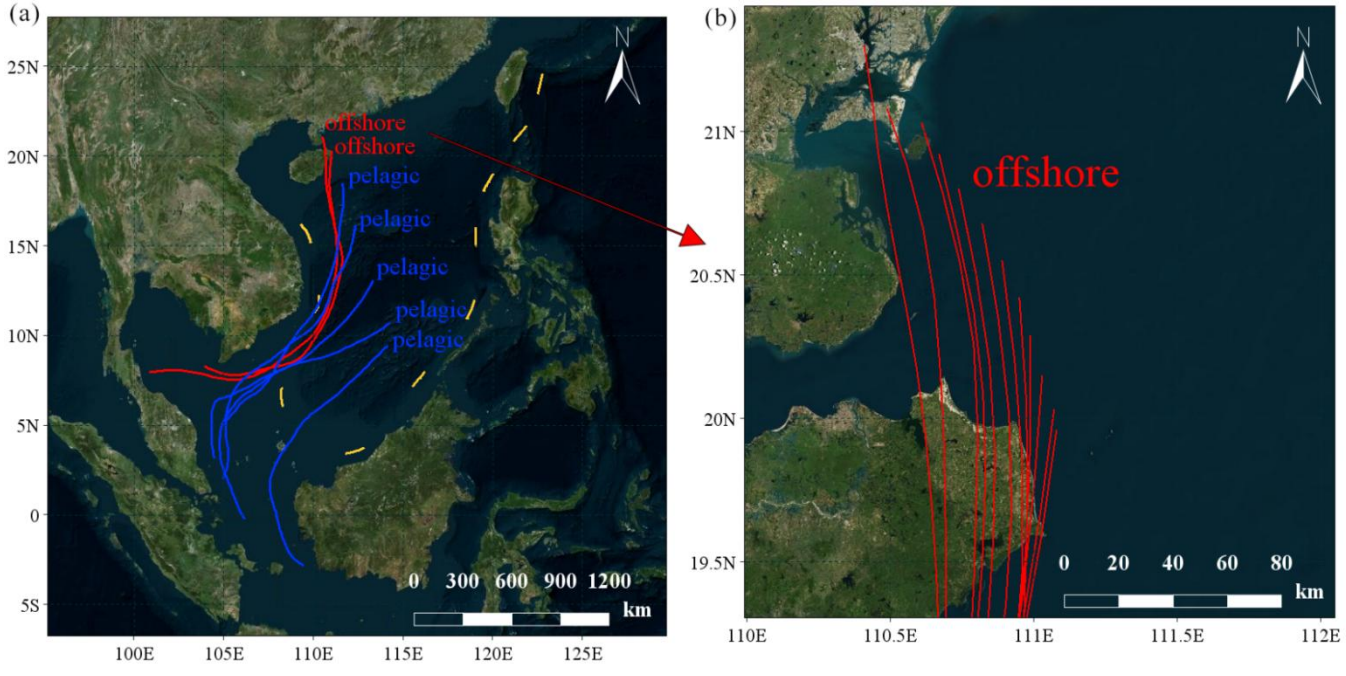

Fig. 8 (a) The 72-h backward trajectory air mass source traces in the offshore (orange solid lines) and pelagic (blue solid lines) regions. (b) Detailed map of the backward trajectory air mass source traces passing through the mainland areas (© Google Earth).

Table 3

Distributions of NCs for different aerosol particle modes in different ocean regions. Mean and SD, respectively, represent the mean values and standard deviations of the related meteorological parameters.

Observation Area	South China Sea			
Route Location	Offshore Region		Pelagic Region	
Marine Aerosol Parameters	Mean	SD	Mean	SD
Accumulation Mode (cm^{-3})	105.57	25.52	47.65	31.63
Coarse Mode (cm^{-3})	2.68	0.38	1.57	0.80
Total (cm^{-3})	108.25	25.43	49.22	31.97
Accumulation Mode / Total (%)	97.52	-	96.81	-
Coarse Mode / Total (%)	2.48	-	3.19	-

https://doi.org/10.5194/egusphere-2025-1463
Preprint. Discussion started: 28 May 2025

Meteorological Parameters				
WS (m s^{-1})	10.74	1.95	8.64	3.70
RH (%)	91.20	1.72	82.41	3.40
T_{OBS} (℃)	28.19	0.57	29.18	0.87
SST (℃)	27.71	0.37	29.78	0.33

3.3. Diurnal variation of NCs and their affecting factors in pelagic regions

The results of Section 3.2 showed that the distributions and components of marine aerosols in different regions were influenced by ocean productions and emissions, as well as continental transports. Among them, the degree of impact on marine transport and background aerosols caused by continental transport and marine generation sources differ greatly due to the discrepancies in the degree of continental transport and marine biological activities at different distances from the coast. Beyond that, on the one hand, many meteorological parameters, such as WS, T_{2m}, SST, and SST-T_{2m}, might influence the concentration and distribution of marine aerosols. On the other hand, the meteorological parameters had obvious day-night differences. Therefore, we analyzed the diurnal variations of the NCs and the correlations between the NCs and different meteorological parameters in this section. In that the sources of 72-h backward trajectory air masses were from the ocean, we selected those marine aerosol data in the pelagic areas with total marine aerosol NCs not exceeding 120 cm^{-3} to exclude the influence of continental transport. These aerosol data also conformed to the classification method, which was proposed by Saliba (2019) to extract relatively clean marine aerosol data; meanwhile, these NCs distinctly represented the characteristics of the local generation of marine aerosol in these regions.

Fig. 9a showed the diurnal variations of the total mean values of NCs in the pelagic region. To better compare the diurnal variation, we divided the data into different periods according to sunrise and sunset times. Consequently, we selected the sunrise and sunset moments, along with the surrounding one-hour interval, as the transition periods to eliminate the effects of day-to-night transitions. Fig. 9a showed a clear diurnal variation emerged. The variations became readily visible for the accumulation mode, following a definite pattern: the NCs remained falling in the nighttime, and they began steadily rising in the night-to-day transition (NDT) period. Then they remained slightly rising or falling in the daytime, but began to fall steadily in the day-to-night transition (DNT) period. Meanwhile, we also found that the NCs had apparent discrepancies between the daytime and nighttime, and they increased or decreased significantly during the transition periods. The comparisons of the size distributions (Fig. 9b) showed that the NCs of the different periods were evenly distributed in the 0.5 to 2.0 μm diameter range. In addition, the average size distributions for marine aerosols were consistent. The reason for these phenomena was that almost all relatively clean marine aerosols were from the oceans. The NCs of the different aerosol particle modes in the different periods were counted in Fig. 9c, and we can find that the average NCs of the total marine aerosols were significantly different in different periods. Specifically, the total NC was 43.86 cm^{-3} in the nighttime, and 47.06 cm^{-3} in the first transition period (i.e., NDT), but it was 48.99 cm^{-3} in the daytime, and reached the highest (58.56 cm^{-3}) in the second transition period (i.e., DNT). The comparisons of the accumulation modes were consistent with those of the

https://doi.org/10.5194/egusphere-2025-1463
Preprint. Discussion started: 28 May 2025

total NCs. The NC of the accumulation mode was 42.26 cm^{-3} in the nighttime, 45.47 cm^{-3} in the NDT period, 47.33 cm^{-3} in the daytime, and 56.89 cm^{-3} in the DNT period. There were pronounced diurnal NC variations, with maximum differences of 35% observed between daytime, nighttime, and transition periods. However, there were no significant differences in the NCs of the coarse modes between different periods, as mentioned above, which were 1.60 cm^{-3}, 1.58 cm^{-3}, 1.66 cm^{-3}, and 1.68 cm^{-3}, respectively.

To explore the reasons for these differences, we further analyzed the correlation coefficients between the NCs and the meteorological parameters (Fig. 10a), suggesting that the NCs of all aerosol particle modes have positive correlations to the WSs. The correlation coefficients were 0.41 for the coarse mode, 0.57 for the accumulation mode, and 0.58 for the total modes. On the contrary, negative correlations between SST and NC were found, which are -0.24, -0.45, and -0.47, respectively, and the NCs were low in the time periods with high SST. Compared to the WS and SST, our results showed that the SST-T_{2m} has a more significant negative correlation with the NCs, with correlation coefficients of -0.30, -0.82, and -0.83. Fig. 10b showed that the WS was lower during the nighttime, and the SST and SST-T_{2m} values were greater, so the NCs were lower than those in the daytime. In the NDT period, the WS did not change significantly, but an obvious decrease in the SST and SST-T_{2m} was found, ultimately resulting in a noticeable increase in the NCs. In this period, the SST and SST-T_{2m} were the dominant factors. However, in the DNT period, the NCs were highest due to the lowest values of SST and SST-T_{2m} and the highest WS. In this period, the significant reduction in WS led to a decrease in the NC. From the above analysis, the meteorological parameters have a joint impact on the production and distribution of marine aerosols.

https://doi.org/10.5194/egusphere-2025-1463
Preprint. Discussion started: 28 May 2025

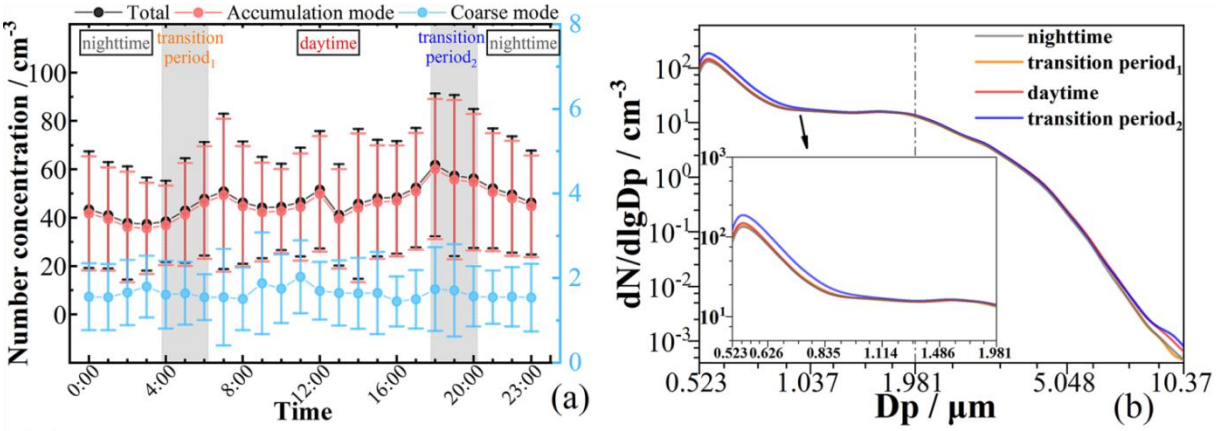

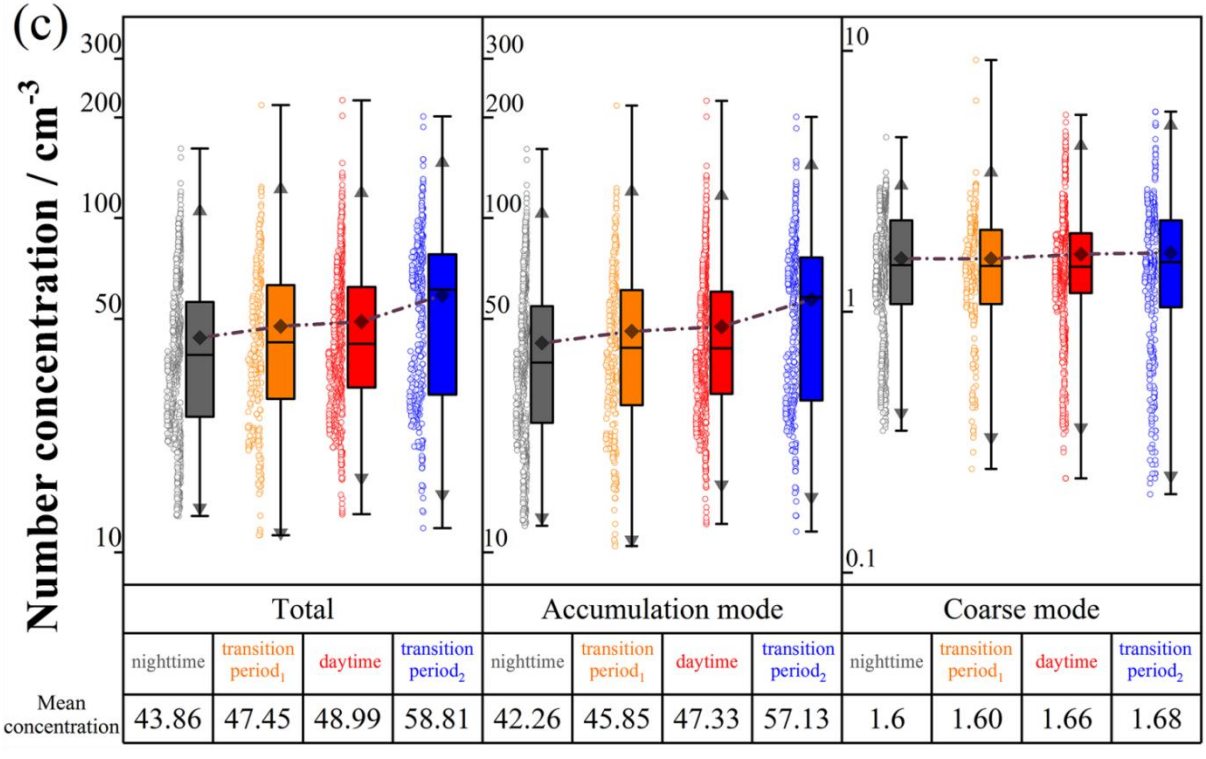

	Total				Accumulation mode				Coarse mode			
	nighttime	transition period$_1$	daytime	transition period$_2$	nighttime	transition period$_1$	daytime	transition period$_2$	nighttime	transition period$_1$	daytime	transition period$_2$
Mean concentration	43.86	47.45	48.99	58.81	42.26	45.85	47.33	57.13	1.6	1.60	1.66	1.68

Fig. 9 (a) Diurnal variations of the total mean values of the NCs in the different aerosol particle modes. The vertical bars showed the standard errors (the shadow areas represented the transition periods between daytime and nighttime). (b) The NCs of average size distributions for marine aerosols of 0.5 to 10 μm diameters in different time periods. (c) The NCs of the different aerosol particle modes in different time periods. For the box plots, the boxes represented the 25th to 75th percentile value, the black whisker represented the maximum and minimum range, the black triangle represented the 1.5 inter-quartile range, the black diamond marker represented the mean value, and the black horizontal line represented the median value.

https://doi.org/10.5194/egusphere-2025-1463
Preprint. Discussion started: 28 May 2025

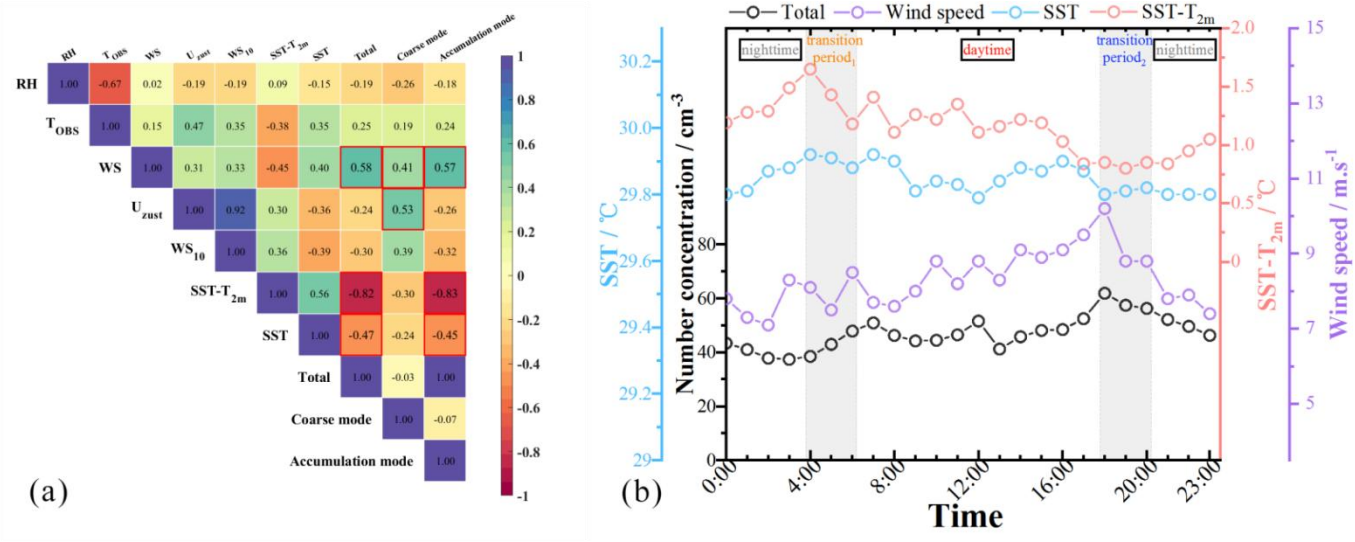

Fig. 10 (a) The correlation coefficients between the NCs of all aerosol particle modes and different meteorological parameters. Correlation plot showing the Pearson correlation values of all marine aerosol NCs and meteorological parameters measured in pelagic regions. (b) The comparisons between the diurnal variations of total NCs, SST, SST-T_{2m}, and WS.

3.3.1. Influence of the WS on marine aerosol NCs

Our measurement results provided robust evidence for the wind-driven marine aerosol production mechanism in the pelagic region. In all SST intervals, we can observe an obvious positive correlation between the WS and the NCs of all aerosol particle modes (Fig. 11), with R values greater than 0.8. In the pelagic region, the NCs were strongly influenced by the local productions and had a relatively short lifetime. Under the influence of sea surface wind, the ocean wave fluctuations increased; meanwhile, the frictions of the sea surface intensified with the actions of the wind stresses. The air bubbles generated and existed on the sea surface, which subsequently ruptured to form lots of water droplets and then produced the primary marine aerosol after evaporation and crystallization processes (Blanchard et al., 1980; Saliba et al., 2019). Therefore, under the WS increased accompanied by synergistic influences of the gas-to-particle conversion and sea surface wind physical friction, the NCs increased in the pelagic region.

https://doi.org/10.5194/egusphere-2025-1463
Preprint. Discussion started: 28 May 2025

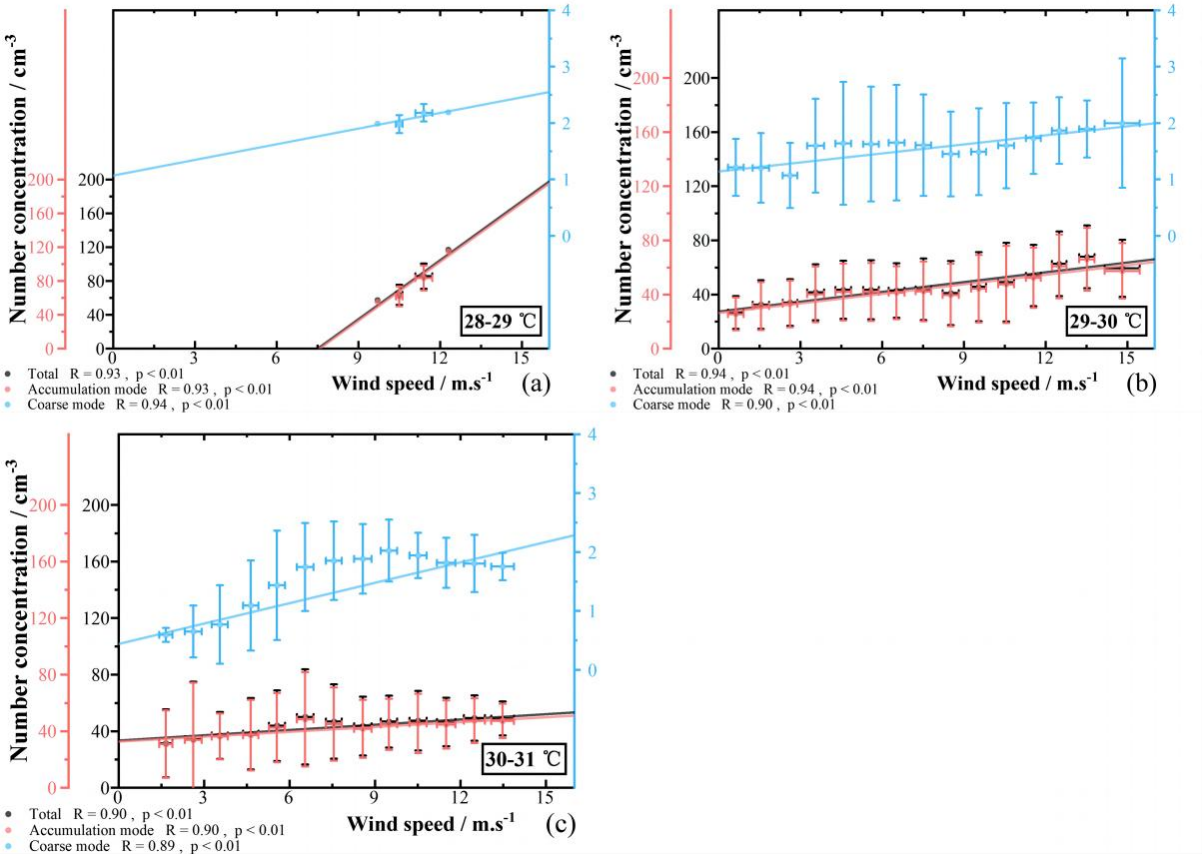

Fig. 11 The NCs versus WS in the pelagic region. The NC of all aerosol particle modes versus WS for 28-29 ℃ (a), 29-30 ℃ (b), and 30-31 ℃ (c) SST intervals. The error bars represented the standard deviations. The R represented the Pearson correlation coefficients, and the p values were performed to test whether the correlations were significant.

3.3.2. Influence of the SST and SST-T_{2m} on marine aerosol NCs

Although the WS can partly explain the variability of the NCs, the NCs exhibited a more obvious negative dependence on SST in all WS intervals. To analyze how SST influenced the NCs in the pelagic region, Fig. 12 showed the NC of all aerosol particle modes versus SST in the WS intervals, in which the WS was approximately constant. It may largely exclude the influences of the WS on the NC. We found a negative correlation between the SST and the NCs for the WS of 0-15 m s^{-1} in the SCS, with their R values being all smaller than -0.75 (Fig. 12). With the comparisons of the regression slopes across the different aerosol particle modes, the SST was likely more sensitive to the accumulation mode. The result was consistent with the previous studies (Salter et al., 2014; Zábori et al., 2012b) but inconsistent with some laboratory studies (Keene et al., 2017; Forestieri et al., 2018). However, a recent study showed that the NCs decreased with the SST (Christiansen et al., 2019). These comparisons suggested that the influences of the SST on the NCs might be different in different seas due to the

https://doi.org/10.5194/egusphere-2025-1463
Preprint. Discussion started: 28 May 2025

different components of the seawater. In the pelagic region of the SCS, according to the results of the previous studies and this study, we inferred that the volume of the air entrained might have decreased as the SST was increased, resulting in the decrease of the plunging jet. Meanwhile, the processes of the bubble rupture changed; the daughter bubbles of smaller diameters were generated at the edges of the central bubbles when the central bubbles ruptured at the sea surface. The generations of the daughter bubbles decreased with the increasing ratio of density to viscosity and the decreasing ratio of viscosity to surface tension; however, the ratio of density to viscosity might increase and ratio of viscosity to surface tension might decrease under the increasing SST, and the number of the sea surface bubbles decrease (Miguet et al., 2021; Sellegri et al., 2023). Therefore, these factors might ultimately result in decreased marine aerosol NCs, especially for the accumulation aerosol mode, with the increasing SST in the SCS.

Compared to the WS and SST, the SST-T_{2m} can better reflect the variations of the NCs ($R > 0.90$, Fig. 13). Meanwhile, Fig. 13 indicated that the NCs had a significant negative correlation with the SST-T_{2m}. Figs. 13 and 14 illustrated the NC of all aerosol particle modes versus SST-T_{2m} in the WS and SST intervals, respectively. In the WS and SST intervals, we found a significant negative correlation between the SST-T_{2m} and the NCs in the SCS (Fig. 14). The SST-T_{2m} was the major determinant of the atmospheric stability, simultaneously playing a relatively important role in the processes of the air convection and mechanical mixing over the ocean (Lewis et al., 2004). With increased SST-T_{2m}, the plume rise phenomenon and the upward transport of marine aerosols might intensify (Yuan et al., 2019). The gravity had little influence on the vertical motion of the small marine aerosol particles; for instance, the marine aerosols with 1 μm diameters needed nearly 24 hours to fall 10 meters in the still air. Hence, the NCs may decrease on the sea surface due to vertical transport. Moreover, the SST-T_{2m} probably influenced the marine aerosol generation by affecting atmospheric stability and thus the interfacial and effective production fluxes of marine aerosols by affecting the sea state, sea wave, and the process of the whitecap formation (Lewis et al., 2004; Song et al., 2023). These phenomena might be an important factor affecting the differences in the marine aerosol NC distributions; meanwhile, they might be important for the abovementioned different conclusions of the previous studies on the relationship between the SST and NCs. The differences in the SST-T_{2m} might cause the inter-study differences despite the consistent SST during the experiment. The specific reasons needed to be further proved by the subsequent targeted research. In summary, the SST-T_{2m} might influence the marine aerosol transport and generation processes, resulting in differences in NCs. Hence, the SST-T_{2m} may be a new and significant parameter to better quantify the impact on the marine aerosol transports and generations in the SCS.

https://doi.org/10.5194/egusphere-2025-1463
Preprint. Discussion started: 28 May 2025

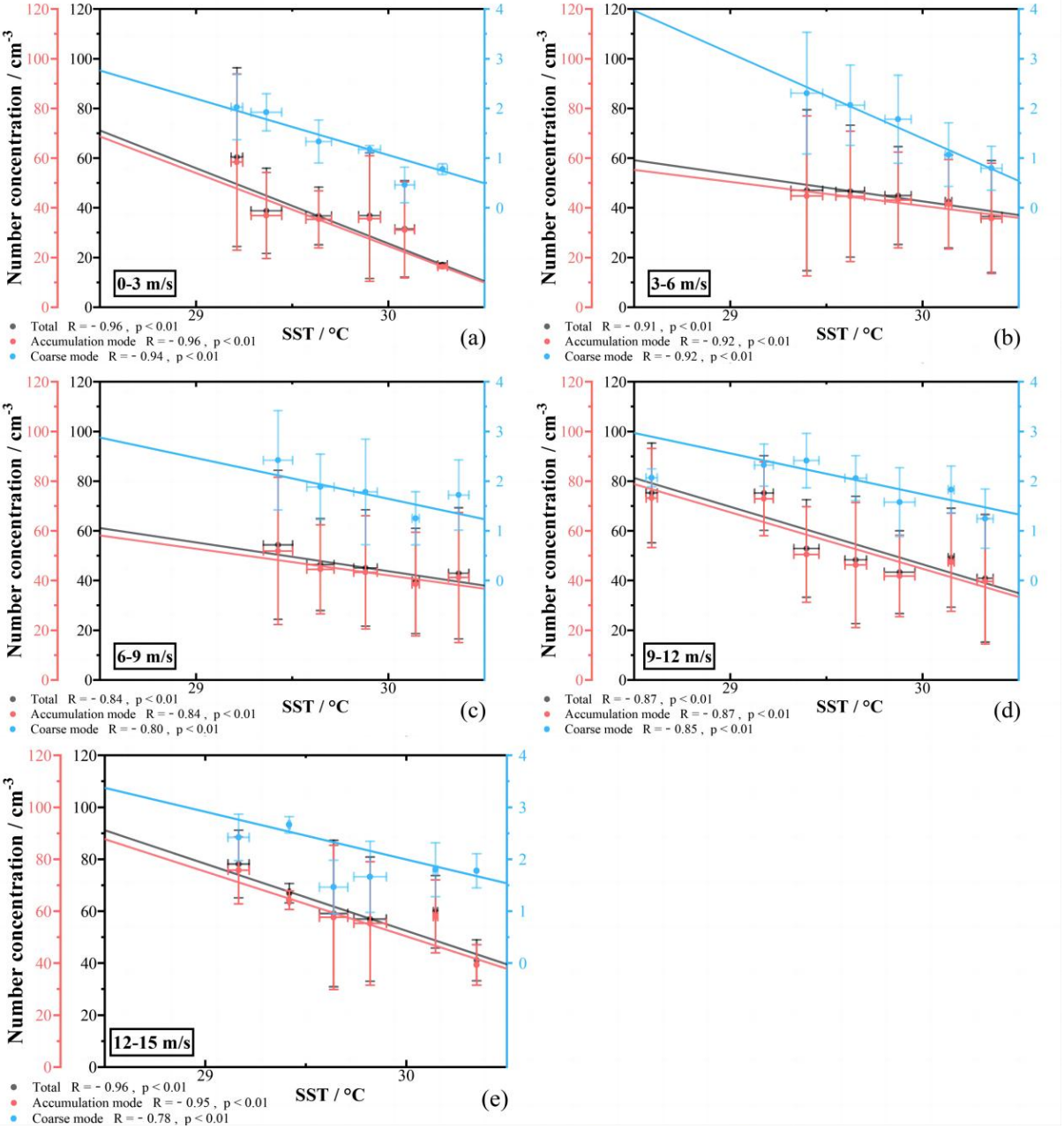

Fig. 12 The NCs versus SST in the pelagic region. The NC of all aerosol particle modes versus SST for 0-3 m s^{-1} (a), 3-6 m s^{-1} (b), 6-9 m s^{-1} (c), 9-12 m s^{-1} (d), and 12-15 m s^{-1} (e) WS intervals. The error bars represented the standard deviations. The R represented the Pearson correlation coefficients, and the p values were performed to test whether the correlations were significant.

https://doi.org/10.5194/egusphere-2025-1463
Preprint. Discussion started: 28 May 2025

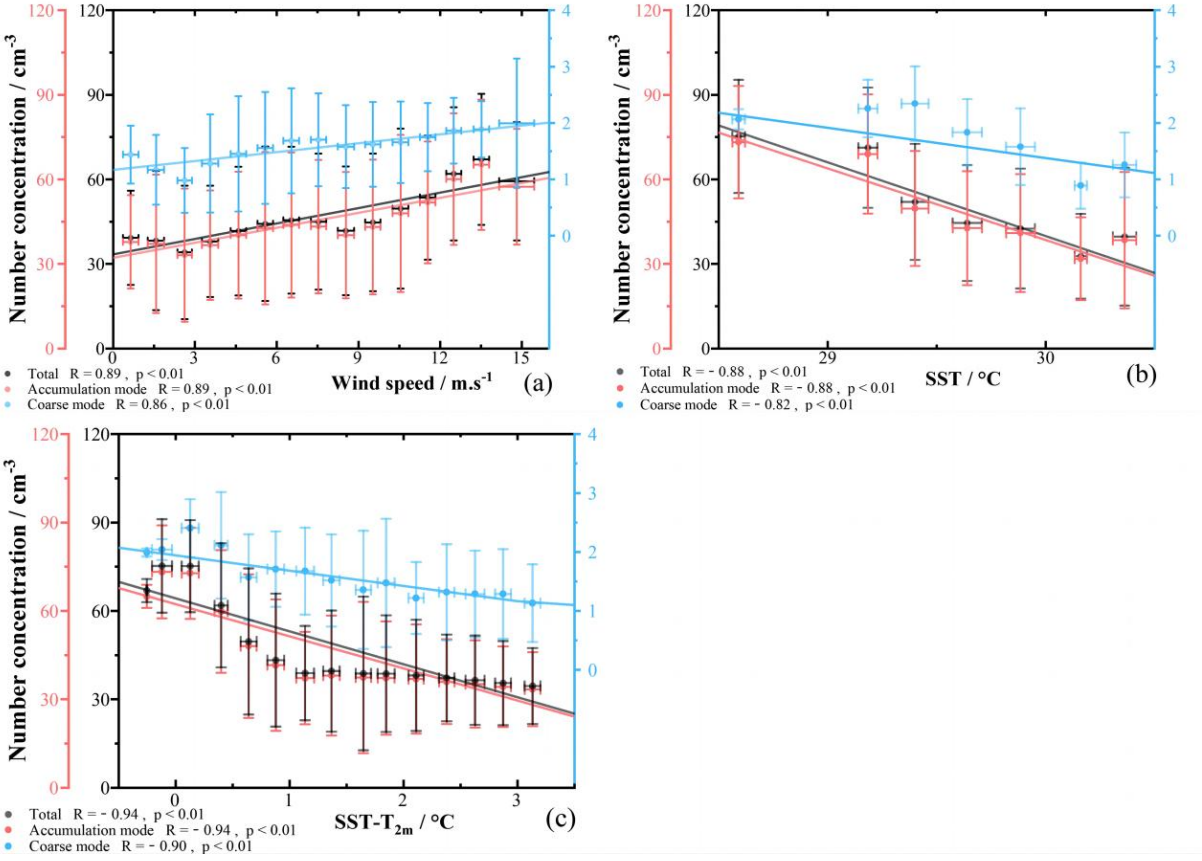

Fig. 13 The relationship between the NC of all aerosol particle modes and WS (a), SST (b), and SST-T_{2m} (c). The error bars represented the standard deviations. The R represented the Pearson correlation coefficients, and the p values were performed to test whether the correlations were significant.

https://doi.org/10.5194/egusphere-2025-1463
Preprint. Discussion started: 28 May 2025

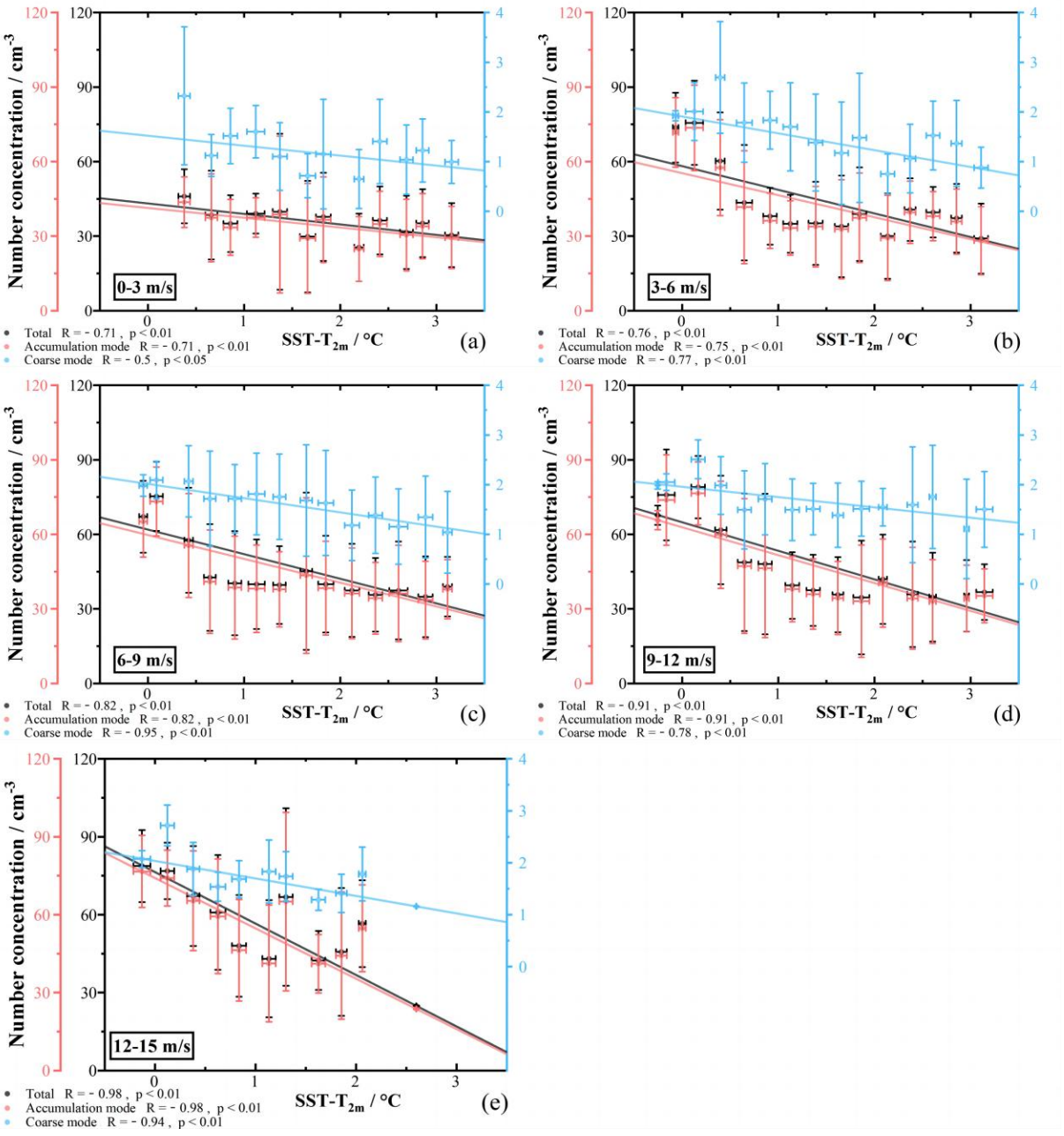

Fig. 14 The NCs versus SST-T_{2m} in the pelagic region. The NC of all aerosol particle modes versus SST-T_{2m} for 0-3 m s^{-1} (a), 3-6 m s^{-1} (b), 6-9 m s^{-1} (c), 9-12 m s^{-1} (d), and 12-15 m s^{-1} (e) WS intervals. The error bars represented the standard deviations. The R represented the Pearson correlation coefficients, and the p values were performed to test whether the correlations were significant.

https://doi.org/10.5194/egusphere-2025-1463
Preprint. Discussion started: 28 May 2025

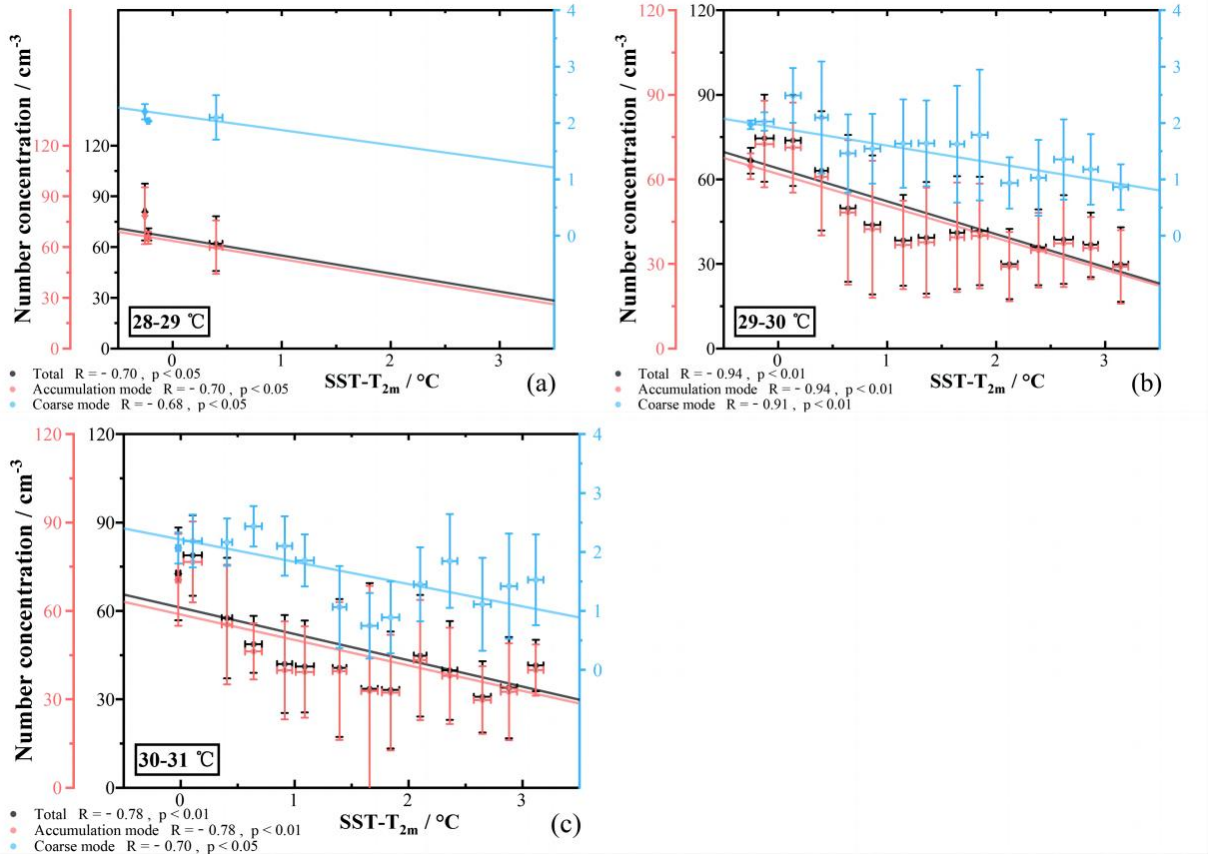

Fig. 15 The NCs versus SST-T_{2m} in the pelagic region. The NC of all aerosol particle modes versus SST-T_{2m} for 28-29 ℃ (a), 29-30 ℃ (b), and 30-31 ℃ (c) SST intervals. The error bars represented the standard deviations. The R represented the Pearson correlation coefficients, and the p values were performed to test whether the correlations were significant.

4. Conclusions

This study utilized cruise-based observational data collected from 21 May to 15 June 2023 to examine marine aerosol NCs and components within the data-sparse SCS. Measurements revealed NCs for the total, accumulation, and coarse modes of 54.01 ± 35.37 cm^{-3}, 52.35 ± 34.96 cm^{-3}, and 1.66 ± 0.83 cm^{-3}, respectively. Analysis of marine aerosol size distributions (0.5–10 μm diameter) exhibited a bimodal structure, with modes at 0.542 μm and 1.981 μm. Spatial characterization of NCs and aerosol components between offshore and pelagic regions revealed distinct differences, demonstrating that distance from the coast significantly influences distributions due to variations in aerosol transport and generation. Furthermore, meteorological parameters, particularly SST-T_{2m}, were proved to potentially induce changes in the transport and generation processes, ultimately leading to discrepancies in the NCs. Diurnal cycles in meteorological parameters also drove pronounced aerosol NC variations, especially during daytime-nighttime transitions. Collectively, these findings proved key explanations of spatiotemporal marine aerosol variations in the SCS and the potential affecting factors.

https://doi.org/10.5194/egusphere-2025-1463
Preprint. Discussion started: 28 May 2025

The result obtained in the SCS demonstrated that the distributions of marine aerosol NCs and components depended on the distances from the coast. In offshore regions, aerosol components were strongly influenced by anthropogenic activities and continental transport processes, with elevated NCs and higher proportions of continental aerosol components (DUST) compared to pelagic regions. Furthermore, NCs exhibited a negative correlation with distance from the coast, consistent with diminishing continental aerosol contributions. Conversely, marine-derived components (SEAS and DMS) dominated in pelagic regions, reflecting intensified marine aerosol production mechanisms.

The influences of meteorological parameters on marine aerosols differed in the pelagic region. Increasing sea surface wind speed (WS) likely drove ocean wave fluctuations and heightened sea surface friction, promoting aerosol particle generation. Conversely, rising sea surface temperature (SST) could reduce plunging jet intensity and entrapped air volume, potentially altering bubble rupture processes and decreasing NCs. Notably, the SST-T_{2m} anomaly exhibited the strongest correlation with NCs. Higher SST-T_{2m} likely reduced interfacial and effective aerosol production fluxes while intensifying vertical transport, collectively lowering NCs. WS, SST, and SST-T_{2m} displayed distinct diurnal cycles. They drove a distinct diurnal variation of NCs, with higher NCs in the daytime than in the nighttime. Meanwhile, during daytime-nighttime transition periods, the variations of NCs emerged as an apparent transition. At night, lower WS combined with higher SST and SST-T_{2m} minimized NCs. Rapid solar radiation shifts drove abrupt meteorological changes during sunrise and sunset, triggering NC fluctuations. In the NDT transition (the transition $period_1$), stable WS left SST and SST-T_{2m} as dominant NC regulators. In the DNT transition (the transition $period_2$), all the aforementioned three factors jointly influenced NCs.

Overall, this study gaps in and updated observational data for the SCS while comprehensively analyzing marine aerosol diurnal variations, continental transport impacts, and future investigated the potential factors, especially the SST-T_{2m} of the meteorological parameters. This finding enables subsequent refinement of traditional marine aerosol generation functions, which rely solely on WS and SST. However, the short-duration cruise data limited robust theoretical conclusions about SST and SST-T_{2m} effects on aerosols. Additionally, validating sea surface phenomena (e.g., whitecap coverage, an indicator of wave-driven aerosol production) against meteorological parameters remained challenging due to scarce on-site observations. Thus, more detailed observations and laboratory experiments were critical in future studies to validate the proposed meteorological element influences and specific mechanisms on aerosol generation and transport.

Data Availability

All data from this research are available from the corresponding author upon request.

https://doi.org/10.5194/egusphere-2025-1463
Preprint. Discussion started: 28 May 2025

Author contributions

SC and TL designed this study. ZQ and HX performed the measurments during the cruise. MZ and YP implemented the back trajectory analysis. ZQ, XL, ZZ and SC analyzed the data. ZQ, SC and XW wrote the paper. All co-authors proofread and commented on the paper.

Competing interests

The authors declare that they have no known competing financial interests or personal relationships that could have appeared to influence the work reported in this paper.

Disclaimer

Publisher's note: Copernicus Publications remains neutral with regard to jurisdictional claims made in the text, published maps, institutional affiliations, or any other geographical representation in this paper. While Copernicus Publications makes every effort to include appropriate place names, the final responsibility lies with the authors.

Acknowledgments

The authors acknowledge the South China Sea Institute of Oceanology, Chinese Academy of Sciences for supporting this research cruise. The authors thank Kun Zhang and Haoda Yang for helping install the instruments. The authors thank the Max-Planck Society for the provision of the PLC model used in this study. The authors thank the NOAA ARL for the provision of the HYSPLIT transport and dispersion model used in this study. The ERA5 hourly dataset used in this study was provided by the ECMWF, and the MERRA-2 dataset was provided by the GMAO at NASA Goddard Space Flight Center.

Financial support

This study was funded by the Strategic Priority Research Program of Chinese Academy of Sciences (No. XDA17010104), Key Scientific Research Project of Anhui Education Department (No.2022AH051712), and Scientific Research Foundation for the Advanced Talents, Chaohu University (No. KYQD-202208).

https://doi.org/10.5194/egusphere-2025-1463
Preprint. Discussion started: 28 May 2025

References

Alexander, B., Park, R. J., Jacob, D. J., Li, Q. B., Yantosca, R. M., Savarino, J., Lee, C. C. W., and Thiemens, H.: Sulphate formation in sea-salt aerosols: Constraints from oxygen isotopes, J. Geophys. Res., 110, D1037, https://doi.org/10.1029/2004jd005659, 2005.

Andreas, E. L.: A new sea spray generation function for wind speeds up to 32 m s^{-1}, J. Phys. Oceanogr., 28, 2175–2184, https://doi.org/10.1175/1520-0485(1998)028<2175:ANSSGF>2.0.CO;2, 1998.

Andreas, E. L.: A review of spray generation function for the open ocean, in: Atmosphere–Ocean Interactions. edited by: Perrie, W. WTT Press, Billerica, Mass, 1–46, 2002.

Andreas, E. L.: Spray-mediated enthalpy flux to the atmosphere and salt flux to the ocean in high winds, J. Phys. Oceanogr., 40, 608–619, https://doi.org/10.1175/2009JPO4232.1., 2010.

Andreae, M. O., and Rosenfeld, D.: Aerosol-cloud-precipitation interactions. Part 1. The nature and sources of cloud-active aerosols, Earth-sci. Rev., 89, 13–41, https://doi.org/10.1016/j.earscirev.2008.03.001, 2008.

Athanasopoulou, E., Protonotariou, A., Papangelis, G., Tombrou, M., and Gerasopoulos, E.: Long-range transport of Saharan dust and chemical transformations over the Eastern Mediterranean, Atmos. Environ., 140, 592–604, https://doi.org/10.1016/j.atmosenv.2016.06.041, 2016.

Atlas, E. and Giam, C. S.: Ambient Concentration and Precipitation Scavenging of Atmospheric Organic Pollutants, Water Air Soil Poll., 38, 19–36, 1988.

Bauer, S. E., Tsigaridis, K., Faluvegi, G., Kelley, M., Lo, K. K., Miller, R. L., Nazarenko, L., Schmidt, G. A., and Wu, J. B.: Historical (1850–2014) aerosol evolution and role on climate forcing using the GISS ModelE2.1 contribution to CMIP6, J. Adv. Model Earth Sy., 12, e2019MS001978, https://doi.org/10.1029/2019MS001978, 2020.

Bird, J. C., de Ruiter, R., Courbin, L., and Stone, H. A.: Daughter bubble cascades produced by folding of ruptured thin films, Nature, 465,759-762, https://doi.org/10.1038/nature09069, 2010.

Blanchard, D. C., and Woodcock, A. H.: The production, concentration, and vertical distribution of the sea-salt aerosol, Ann. N. Y. Acad. Sci., 338, 330–347, https://doi.org/10.1111/j.1749-6632.1980.tb17130.x, 1980.

Bruch, W., Yohia, C., Tulet, P., Limoges, A., Sutherland, P., van Eijk, A. M. J., Missamou, T. and Piazzola, J.: Atmospheric sea spray modeling in the North-East Atlantic Ocean using tunnel-derived generation functions and the SUMOS cruise data set, J. Geophys. Res.-Atmos., 128, e2022JD038330, https://doi.org/10.1029/2022JD038330, 2023.

Bzdek, B. R., Reid, J. P., and Cotterell, M. I.: Open questions on the physical properties of aerosols, Comm. Chem., 3, 105, https://doi.org/10.1038/s42004-020-00342-9, 2020.

Cai, M., Liang, B. L., Sun, Q. B., Zhou, S. Z., Chen, X. Y., Yuan, B., Shao, M., Tan, H. B., and Zhao, J.: Effects of continental emissions on cloud condensation nuclei (CCN) activity in the northern South China Sea during summertime 2018, Atmos. Chem. Phys., 20, 9153–9167, https://doi.org/10.5194/acp-20-9153-2020, 2020.

https://doi.org/10.5194/egusphere-2025-1463
Preprint. Discussion started: 28 May 2025

Carslaw, K. S., Boucher, O., Spracklen, D. V., Mann, G. W., Rae, J. G. L., Woodward, S., and Kulmala, M.: A review of natural aerosol interactions and feedbacks within the Earth system, Atmos. Chem. Phys., 10, 1701–1737, https://doi.org/10.5194/acp-10-1701-2010, 2010.

Chen, S. P., Lu, C. H., Queen, J. M., and Lee, P.: Application of satellite observations in conjunction with aerosol reanalysis to characterize long-range transportof African and Asian dust on air quality in the contiguous U.S, Atmos. Environ., 187, 174–195, https://doi.org/10.1016/j.atmosenv.2018.05.038, 2018.

Christiansen, S., Salter, M. E., Gorokhova, E., Nguyen, Q. T., and Bilde, M.: Sea spray aerosol formation: Laboratory results on the role of air entrainment, water temperature, and phytoplankton biomass, Environ. Sci. Technol., 53, 13107–13116, https://doi.org/10.1021/acs.est.9b04078, 2019.

Decesari, S., Finessi, E., Rinaldi, M., Paglione, M., Fuzzi, S., Stephanou, E. G., Tziaras, T., Spyros, A., Ceburnis, D., O'Dowd, C., Dall'Osto, M., Harrison, R. M., Allan, J., Coe, H., and Facchini, M. C.: Primary and secondary marine aerosols over the North Atlantic Ocean during the MAP experiment, J. Geophys. Res., 116, 1–21, https://doi.org/10.1029/2011JD016204, 2011.

Duce, R. A., Winchester, J. W., and Van Nahl, T. W.: Iodine, bromine, and chlorine in the Hawaiian marine atmosphere, J. Geophys. Res., 70, 1775–1799, https://doi.org/10.1029/JZ070i008p01775, 1965.

Ehn, M., Vuollekoski, H., Petäjä, T., Kerminen, V.-M., Vana, M., Aalto, P., de Leeuw, G., Ceburnis, D., Dupuy, R., O'Dowd, C. D., and Kulmala, M.: Growth rates during coastal and marine new particle formation in western Ireland, J. Geophys. Res.-Atmos., 115, https://doi.org/10.1029/2010JD014292, 2010.

Eriksson, E.: The yearly circulation of chloride and sulfur in nature: Meteorological, geochemical and pedological implications. Part II, Tellus, 11, 375-403, https://doi.org/10.1111/j.2153-3490.1960.tb01284.x, 1960.

Feingold, G., Cotton, W. R., Kreidenweis, S. M., and Davis, J. T.: The Impact of Giant Cloud Condensation Nuclei on Drizzle Formation in Stratocumulus: Implications for Cloud Radiative Properties, J. Atmos. Sci., 56, 4100-4117, https://doi.org/10.1175/1520-0469(1999)056<4100:TIOGCC>2.0.CO;2, 1999.

Flores, J. M., Bourdin, G., Altaratz, O., Trainic, M., Lang-Yona, N., Dzimban, E., Steinau, S., Tettich, F., Planes, S., Allemand, D., Agostini, S., Banaigs, B., Boissin, E., Boss, E., Douville, E., Forcioli, D., Furla, P., Galand, P. E., Sullivan, M. B., Gilson, É., Lombard, F., Moulin, C., Pesant, S., Poulain, J., Reynaud, S., Romac, S., Sunagawa, S., Thomas, O. P., Troublé, R., de Vargas, C., Thurber, R. V., Voolstra, C. R., Wincker, P., Zoccola, D., Bowler, C., Gorsky, G., Rudich, Y., Vardi, A., and Koren, I.: Tara Pacific Expedition's Atmospheric Measurements of Marine Aerosols across the Atlantic and Pacific Oceans: Overview and Preliminary Results, Bull. Am. Meteorol. Soc., 101, E536-E554, https://doi.org/10.1175/BAMS-D-18-0224.1, 2020.

Forestieri, S. D., Moore, K. A., Martinez Borrero, R., Wang, A., Stokes, M. D., and Cappa, C. D.: Temperature and Composition Dependence of Sea Spray Aerosol Production, Geophys. Res. Lett., 45, 7218-7225, https://doi.org/10.1029/2018GL078193, 2018.

https://doi.org/10.5194/egusphere-2025-1463
Preprint. Discussion started: 28 May 2025

Gathman, S. G.: Optical Properties Of The Marine Aerosol As Predicted By The Navy Aerosol Model, Opt. Eng., 22, 220157, 1983.

Global Modeling and Assimilation Office (GMAO): MERRA-2 tavg1_2d_aer_Nx: 2d,1-Hourly,Time-averaged,Single-Level,Assimilation,Aerosol Diagnostics V5.12.4, Greenbelt, MD, USA, Goddard Earth Sciences Data and Information Services Center (GES DISC) [data set], https://doi.org/10.5067/7MCPBJ41Y0K6, 2015.

Han, S., Cai, Z., Liu, J., Zhang, M., Chen, J., and Lin, Y.: Comparison on aerosol physicochemical properties of sea and land along the coast of Bohai, China, Sci. Total Environ., 673, 148-156, https://doi.org/10.1016/j.scitotenv.2019.04.040, 2019.

Hersbach, H., Bell, B., Berrisford, P., Biavati, G., Horányi, A., Muñoz Sabater, J., Nicolas, J., Peubey, C., Radu, R., Rozum, I., Schepers, D., Simmons, A., Soci, C., Dee, D., and Thépaut, J.-N.: ERA5 monthly averaged data on single levels from 1940 to present, https://doi.org/10.24381/cds.f17050d7, 2023.

Hoppel, W. A.: Measurement of the Size Distribution and CCN Supersaturation Spectrum of Submicron Aerosols over the Ocean, J. Atmos. Sci., 36, 2006-2015, https://doi.org/10.1175/1520-0469(1979)036<2006:MOTSDA>2.0.CO;2, 1979.

Hoppel, W. A., Fitzgerald, J. W., and Larson, R. E.: Aerosol size distributions in air masses advecting off the east coast of the United States, J. Geophys. Res.-Atmos., 90, 2365-2379, https://doi.org/10.1029/JD090iD01p02365, 1985.

Irshad, R., Grainger, R. G., Peters, D. M., McPheat, R. A., Smith, K. M., and Thomas, G.: Laboratory measurements of the optical properties of sea salt aerosol, Atmos. Chem. Phys., 9, 221-230, https://doi.org/10.5194/acp-9-221-2009, 2009.

Jaeglé, L., Quinn, P. K., Bates, T. S., Alexander, B., and Lin, J. T.: Global distribution of sea salt aerosols: new constraints from in situ and remote sensing observations, Atmos. Chem. Phys., 11, 3137-3157, https://doi.org/10.5194/acp-11-3137-2011, 2011.

Jiang, B., Xie, Z., Lam, P. K. S., He, P., Yue, F., Wang, L., Huang, Y., Kang, H., Yu, X., and Wu, X.: Spatial and temporal distribution of sea salt aerosol mass concentrations in the marine boundary layer from the Arctic to the Antarctic, J. Geophys. Res.-Atmos., 126, e2020JD033892, https://doi.org/10.1029/2020JD033892, 2021.

Jing, Z., Chang, P., Shan, X., Wang, S., Wu, L., and Kurian, J.: Mesoscale SST dynamics in the Kuroshio–Oyashio extension region, J. Phys. Oceanogr., 49, 1339-1352, https://doi.org/10.1175/JPO-D-18-0159.1, 2019.

Joung, Y., Buie, C.: Aerosol generation by raindrop impact on soil, Nat. Commun., 6, 6083, https://doi.org/10.1038/ncomms7083, 2015.

Keene, W. C., Long, M. S., Reid, J. S., Frossard, A. A., Kieber, D. J., Maben, J. R., Russell, L. M., Kinsey, J. D., Quinn, P. K., and Bates, T. S.: Factors that modulate properties of primary marine aerosol generated from ambient seawater on ships at sea, J. Geophys. Res.-Atmos., 122, 11,961-911,990, https://doi.org/10.1002/2017JD026872, 2017.

Kim, J. H., Yum, S. S., Lee, Y. G., and Choi, B. C.: Ship measurements of submicron aerosol size distributions over the Yellow Sea and the East China Sea, Atmos. Res., 93, 700-714, https://doi.org/10.1016/j.atmosres.2009.02.011, 2009.

Kong, Y. W., Sheng, L. F., Liu, Q., and Li, X. Z.: Impact of marine atmospheric process on aerosol number size distribution in the South China Sea, (in Chinese), Environ. Sci., 37, 2443-2452, 10.13227/j.hjkx.2016.07.005, 2016.

https://doi.org/10.5194/egusphere-2025-1463
Preprint. Discussion started: 28 May 2025

Korhonen, H., Carslaw, K. S., Spracklen, D. V., Mann, G. W., and Woodhouse, M. T.: Influence of oceanic dimethyl sulfide emissions on cloud condensation nuclei concentrations and seasonality over the remote Southern Hemisphere oceans: a global model study, J. Geophys. Res.-Atmos., 113, 1–16, https://doi.org/10.1029/2007JD009718, 2008.

Kuang, C., McMurry, P. H., and McCormick, A. V.: Determination of cloud condensation nuclei production from measured new particle formation events, Geophys. Res. Lett., 36, https://doi.org/10.1029/2009GL037584, 2009.

Lawler, M. J., Sander, R., Carpenter, L. J., Lee, J. D., von Glasow, R., Sommariva, R., and Saltzman, E. S.: HOCl and Cl2 observations in marine air, Atmos. Chem. Phys., 11, 7617-7628, 10.5194/acp-11-7617-2011, 2011.

Leck, C. and Persson, C.: Seasonal and short-term variability in dimethyl sulfide, sulfur dioxide and biogenic sulfur and sea salt aerosol particles in the arctic marine boundary layer during summer and autumn, Tellus B, 48, 272–299, https://doi.org/10.3402/tellusb.v48i2.15891, 1996.

Levin, Z., Teller, A., Ganor, E., and Yin, Y.: On the interactions of mineral dust, sea-salt particles, and clouds: A measurement and modeling study from the Mediterranean Israeli Dust Experiment campaign, J. Geophys. Res.-Atmos., 110, D20202, https://doi.org/10.1029/2005JD005810, 2005.

Lewis, E. and Schwartz, S.: Sea Salt Aerosol Production: Mechanisms, Methods, Measurements and Models—A Critical Review, Washington DC American Geophysical Union Geophysical Monograph Series, 152, 3719, 10.1029/GM152, 2004.

Li, J., Carlson, B. E., Yung, Y. L., Lv, D., Hansen, J., Penner, J. E., Liao, H., Ramaswamy, V., Kahn, R. A., Zhang, P., Dubovik, O., Ding, A., Lacis, A. A., Zhang, L., and Dong, Y.: Scattering and absorbing aerosols in the climate system, Nat. Rev. Earth Environ., 3, 363-379, 10.1038/s43017-022-00296-7, 2022.

Lin, P., Hu, M., Wu, Z., Niu, Y., and Zhu, T.: Marine aerosol size distributions in the springtime over China adjacent seas, Atmos. Environ., 41, 6784-6796, https://doi.org/10.1016/j.atmosenv.2007.04.045, 2007.

Long, M. S., Keene, W. C., Easter, R. C., Sander, R., Liu, X., Kerkweg, A., and Erickson, D.: Sensitivity of tropospheric chemical composition to halogen-radical chemistry using a fully coupled size-resolved multiphase chemistry–global climate system: halogen distributions, aerosol composition, and sensitivity of climate-relevant gases, Atmos. Chem. Phys., 14, 3397-3425, https://doi.org/10.5194/acp-14-3397-2014, 2014.

Ma, X., Jing, Z., Chang, P., Liu, X., Montuoro, R., Small, R. J., Bryan, F. O., Greatbatch, R. J., Brandt, P., Wu, D., Lin, X., and Wu, L.: Western boundary currents regulated by interaction between ocean eddies and the atmosphere, Nature, 535, 533-537, https://doi.org/10.1038/nature18640, 2016.

Ma, Y., Zhang, X., Xin, J., Zhang, W., Wang, Z., Liu, Q., Wu, F., Wang, L., Lyu, Y., Wang, Q., and Ma, Y.: Mass and number concentration distribution of marine aerosol in the Western Pacific and the influence of continental transport, Environ. Pollut., 298, 118827, https://doi.org/10.1016/j.envpol.2022.118827, 2022.

Mårtensson, E. M., Nilsson, E. D., de Leeuw, G., Cohen, L. H., and Hansson, H.-C.: Laboratory simulations and parameterization of the primary marine aerosol production, J. Geophys. Res.-Atmos., 108, 4297, https://doi.org/10.1029/2002JD002263, 2003.

https://doi.org/10.5194/egusphere-2025-1463
Preprint. Discussion started: 28 May 2025

Meinrat, O.Andreae., and Paul, J.Crutzen.: Atmospheric Aerosols: Biogeochemical Sources and Role in Atmospheric Chemistry, Science, 276, 1052-1058, DOI: 10.1126/science.276.5315.1052, 1997.

Miguet, J., Rouyer, F., and Rio, E.: The Life of a Surface Bubble, Molecules, 26, 1317, https://doi.org/10.3390/molecules26051317, 2021.

Myhre, G., Stordal, F., Johnsrud, M., Ignatov, A., Mishchenko, M. I., Geogdzhayev, I. V., Tanré, D., Deuzé, J.-L., Goloub, P., Nakajima, T., Higurashi, A., Torres, O., and Holben, B.: Intercomparison of Satellite Retrieved Aerosol Optical Depth over the Ocean, J. Atmos. Sci., 61, 499-513, https://doi.org/10.1175/1520-0469(2004)061<0499:IOSRAO>2.0.CO;2, 2004.

Nascimento, J. P., Bela, M. M., Meller, B. B., Banducci, A. L., Rizzo, L. V., Vara-Vela, A. L., Barbosa, H. M. J., Gomes, H., Rafee, S. A. A., Franco, M. A., Carbone, S., Cirino, G. G., Souza, R. A. F., McKeen, S. A., and Artaxo, P.: Aerosols from anthropogenic and biogenic sources and their interactions – modeling aerosol formation, optical properties, and impacts over the central Amazon basin, Atmos. Chem. Phys., 21, 6755–6779, https://doi.org/10.5194/acp-21-6755-2021, 2021.

Nguyen, Q. T., Kjær, K. H., Kling, K. I., Boesen, T., and Bilde, M.: Impact of fatty acid coating on the CCN activity of sea salt particles, Tellus B, 69, 1–15, 1304064, https://doi.org/10.1080/16000889.2017.1304064, 2017.

O'Dowd, C. D. and de Leeuw, G.: Marine aerosol production: a review of the current knowledge, Philos. T. R. Soc. A, 365, 1753-1774, https://doi.org/10.1098/rsta.2007.2043, 2007.

O'Neill, L. W., Chelton, D. B., and Esbensen, S. K.: The effects of SST-induced surface wind speed and direction gradients on midlatitude surface vorticity and divergence, J. Climate, 23, 255-281, https://doi.org/10.1175/2009JCLI2613.1, 2010.

Ovadnevaite, J., Manders, A., de Leeuw, G., Ceburnis, D., Monahan, C., Partanen, A. I., Korhonen, H., and O'Dowd, C. D.: A sea spray aerosol flux parameterization encapsulating wave state, Atmos. Chem. Phys., 14, https://doi.org/10.5194/acp-14-1837-2014, 2014.

Pagels, J., Gudmundsson, A., Gustavsson, E., Asking, L., and Bohgard, M.: Evaluation of aerodynamic particle sizer and electrical low-pressure impactor for unimodal and bimodal mass-weighted size distributions, Aerosol Sci. Tech., 39, 871-887, 2005.

Pant, V., Deshpande, C. G., and Kamra, A. K.: The concentration and number size distribution measurements of the Marine Boundary Layer aerosols over the Indian Ocean, Atmos. Res., 92, 381-393, https://doi.org/10.1016/j.atmosres.2008.12.004, 2009.

Peters, T. M., and Leith D.: Concentration measurement and counting efficiency of the aerodynamic particle sizer 3321, J. Aerosol Sci., 34, 627-634, 2003.

Peters, T. M.: Use of the Aerodynamic Particle Sizer to measure ambient $PM_{10-2.5}$: The coarse fraction of PM_{10}, J. Air Waste Manage., 56, 411-416, 2006.

https://doi.org/10.5194/egusphere-2025-1463
Preprint. Discussion started: 28 May 2025

Prospero, J.M.: Mineral and sea salt aerosol concentrations in various ocean regions, J. Geophys. Res.-Oceans, 84, 725–731, https://doi.org/10.1029/JC084iC02p00725, 1979.

Provençal, S., Buchard, V., da Silva, A. M., Leduc, R., and Barrette, N.: Evaluation of PM surface concentrations simulated by Version 1 of NASA's MERRA Aerosol Reanalysis over Europe, Atmos. Pollut. Res., 8, 374-382, https://doi.org/10.1016/j.apr.2016.10.009, 2017a.

Provençal, S., Buchard, V., Silva, A. M. d., Leduc, R., Barrette, N., Elhacham, E., and Wang, S. H.: Evaluation of PM2.5 Surface Concentrations Simulated by Version 1 of NASA's MERRA Aerosol Reanalysis over Israel and Taiwan, Aerosol Air Qual. Res., 17, 253-261, https://doi.org/10.4209/aaqr.2016.04.0145, 2017b.

Radke, L. F., Hobbs, P. V., and Eltgroth, M. W.: Scavenging of Aerosol Particles by Precipitation, J. Appl. Meteorol., 19, 715–722, 1980.

Sakerin, S. M., Bobrikov, A. A., Bukin, O. A., Golobokova, L. P., Pol'kin, Vas. V., Pol'kin, Vik. V., Shmirko, K. A., Kabanov, D. M., Khodzher, T. V., Onischuk, N. A., Pavlov, A. N., Potemkin, V. L., and Radionov, V. F.: On measurements of aerosol-gas composition of the atmosphere during two expeditions in 2013 along the Northern Sea Route, Atmos. Chem. Phys., 15, 12413–12443, https://doi.org/10.5194/acp-15-12413-2015, 2015.

Saliba, G., Chen, C.-L., Lewis, S., Russell, L. M., Rivellini, L.-H., Lee, A. K. Y., Quinn, P. K., Bates, T. S., Haëntjens, N., Boss, E. S., Karp-Boss, L., Baetge, N., Carlson, C. A., and Behrenfeld, M. J.: Factors driving the seasonal and hourly variability of sea-spray aerosol number in the North Atlantic, P. Natl. Acad. Sci. USA., 116, 20309-20314, https://doi.org/10.1073/pnas.1907574116, 2019.

Salter, M. E., Nilsson, E. D., Butcher, A., and Bilde, M.: On the seawater temperature dependence of the sea spray aerosol generated by a continuous plunging jet, J. Geophys. Res.-Atmos., 119, 9052-9072, https://doi.org/10.1002/2013JD021376, 2014.

Sander, R., Keene, W. C., Pszenny, A. A. P., Arimoto, R., Ayers, G. P., Baboukas, E., Cainey, J. M., Crutzen, P. J., Duce, R. A., Hönninger, G., Huebert, B. J., Maenhaut, W., Mihalopoulos, N., Turekian, V. C., and Van Dingenen, R.: Inorganic bromine in the marine boundary layer: a critical review, Atmos. Chem. Phys., 3, 1301-1336, https://doi.org/10.5194/acp-3-1301-2003, 2003.

Savoie, D. L., Prospero, J. M., Larsen, R. J., Huang, F., Izaguirre, M. A., Huang, T., Snowdon, T. H., Custals, L., and Sanderson, C. G.: Nitrogen and sulfur species in Antarctic aerosols at Mawson, Palmer Station, and Marsh (King George Island), J. Atmos. Chem., 17, 95-122, https://doi.org/10.1007/bf00702821, 1993.

Sellegri, K., O'Dowd, C. D., Yoon, Y. J., Jennings, S. G., and de Leeuw, G.: Surfactants and submicron sea spray generation, J. Geophys. Res.-Atmos., 111, D22215, https://doi.org/10.1029/2005JD006658, 2006.

Sellegri, K., Barthelmeß, T., Trueblood, J., Cristi, A., Freney, E., Rose, C., Barr, N., Harvey, M., Safi, K., Deppeler, S., Thompson, K., Dillon, W., Engel, A., and Law, C.: Quantified effect of seawater biogeochemistry on the temperature dependence of sea spray aerosol fluxes, Atmos. Chem. Phys., 23, 12949-12964, https://doi.org/10.5194/acp-23-12949-2023, 2023.

https://doi.org/10.5194/egusphere-2025-1463
Preprint. Discussion started: 28 May 2025

Smith, M. H., Park, P. M., and Consterdine, I. E.: Marine aerosol concentrations and estimated fluxes over the sea, Q. J. Rol. Meteor. Soc., 119, 809-824, https://doi.org/10.1002/qj.49711951211, 1993.

Solomon, S., Daniel, J. S., Neely, III, R. R., Vernier, J.-P., Dutton, E. G., and Thomason, L. W.: The Persistently Variable "Background" Stratospheric Aerosol Layer and Global Climate Change, Science, 333, 866-870, DOI:10.1126/science.1206027, 2011.

Song, A., Li, J., Tsona, N. T., and Du, L.: Parameterizations for sea spray aerosol production flux, Appl. Geochem., 157, 105776, https://doi.org/10.1016/j.apgeochem.2023.105776, 2023.

Su, Y., Han, Y., Luo, H., Zhang, Y., Shao, S., and Xie, X.: Physical-optical properties of marine aerosols over the South China Sea: shipboard measurements and MERRA-2 reanalysis, Remote Sens., 14, 2453, https://doi.org/10.3390/rs14102453, 2022.

Tang, I. N.: Thermodynamic and optical properties of sea salt aerosol, J. Geophys. Res., 102, 23269–23275, https://doi.org/10.1029/97JD01806, 1997

Textor, C., Schulz, M., Guibert, S., Kinne, S., Balkanski, Y., Bauer, S., Berntsen, T., Berglen, T., Boucher, O., Chin, M., Dentener, F., Diehl, T., Easter, R., Feichter, H., Fillmore, D., Ghan, S., Ginoux, P., Gong, S., Grini, A., Hendricks, J., Horowitz, L., Huang, P., Isaksen, I., Iversen, I., Kloster, S., Koch, D., Kirkevåg, A., Kristjansson, J. E., Krol, M., Lauer, A., Lamarque, J. F., Liu, X., Montanaro, V., Myhre, G., Penner, J., Pitari, G., Reddy, S., Seland, Ø., Stier, P., Takemura, T., and Tie, X.: Analysis and quantification of the diversities of aerosol life cycles within AeroCom, Atmos. Chem. Phys., 6, 1777-1813, https://doi.org/10.5194/acp-6-1777-2006, 2006.

Troitskaya, Y., Kandaurov, A., Ermakova, O., Kozlov, D., Sergeev, D., and Zilitinkevich, S.: The "bag breakup" spume droplet generation mechanism at high winds. Part I: Spray generation functionr, J. Phys. Oceanogr., 48, 2167–2188, https://doi.org/10.1175/jpo-d-17-0104.1, 2018.

von der Weiden, S.-L., Drewnick, F., and Borrmann, S.: Particle Loss Calculator – a new software tool for the assessment of the performance of aerosol inlet systems, Atmos. Meas. Tech., 2, 479–494, https://doi.org/10.5194/amt-2-479-2009, 2009.

Wise, M. E., Freney, E. J., Tyree, C. A., Allen, J. O., Martin, S. T., Russell, L. M., and Buseck, P. R.: Hygroscopic behavior and liquid-layer composition of aerosol particles generated from natural and artificial seawater, J. Geophys. Res.-Atmos., 114, D03201, https://doi.org/10.1029/2008JD010449, 2009.

Woodcock, A. H.: Atmospheric seasalt particles and raindrops, J. Atmos. Sci., 9, 200-212, https://doi.org/10.1175/1520-0469(1952)009<0200:ASPAR>2.0.CO;2, 1952.

Woodcock, A. H.: Salt nuclei in marine air as a function of altitude and wind force, J. Atmos. Sci., 10, 362-371, https://doi.org/10.1175/1520-0469(1953)010<0366:SNIMAA>2.0.CO;2, 1953.

Woods, E., Chung, D., Lanney, H. M., and Ashwell, B. A.: Surface morphology and phase transitions in mixed Nacl/MgSO4 aerosol particles, J. Phys. Chem. A, 114, 2837-2844, https://doi.org/10.1021/jp911133j, 2010.

https://doi.org/10.5194/egusphere-2025-1463
Preprint. Discussion started: 28 May 2025

Yan, J., Lin, Q., Zhang, M. M., Zhao, S. H., and Chen, L. Q.: Effect of air masses motion on the rapid change of aerosols in marine atmosphere, J. Environ. Sci., 83, 217-228, https://doi.org/10.1016/j.jes.2019.04.005, 2019.

Yang, M., Norris, S. J., Bell, T. G., and Brooks, I. M.: Sea spray fluxes from the southwest coast of the United Kingdom–dependence on wind speed and wave height, Atmos. Chem. Phys., 19, 15271-15284, https://doi.org/10.5194/acp-19-15271-2019, 2019.

Yuan, R., Zhang, X., Liu, H., Gui, Y., Shao, B., Tao, X., Wang, Y., Zhong, J., Li, Y., and Gao, Z.: Aerosol vertical mass flux measurements during heavy aerosol pollution episodes at a rural site and an urban site in the Beijing area of the North China Plain, Atmos. Chem. Phys., 19, 12857-12874, https://doi.org/10.5194/acp-19-12857-2019, 2019.

Zábori, J., Matisāns, M., Krejci, R., Nilsson, E. D., and Ström, J.: Artificial primary marine aerosol production: a laboratory study with varying water temperature, salinity, and succinic acid concentration, Atmos. Chem. Phys., 12, 10709-10724, https://doi.org/10.5194/acp-12-10709-2012, 2012a.

Zábori, J., Krejci, R., Ekman, A. M. L., Mårtensson, E. M., Ström, J., de Leeuw, G., and Nilsson, E. D.: Wintertime Arctic Ocean sea water properties and primary marine aerosol concentrations, Atmos. Chem. Phys., 12, 10405-10421, https://doi.org/10.5194/acp-12-10405-2012, 2012b.

Zeng, J., Zhang, G., Long, S., Liu, K., Cao, L., Bao, L., and Li, Y.: Sea salt deliquescence and crystallization in atmosphere: an in situ investigation using x-ray phase contrast imaging, Surf. Interface Anal., 45, 930-936, https://doi.org/10.1002/sia.5184, 2013.

Zhou, K., Wang, S., Lu, X., Chen, H., Wang, L., Chen, J., Yang, X., Wang, X.: Production flux and chemical characteristics of spray aerosol generated from raindrop impact on seawater and soil, J. Geophys. Res.-Atmos., 125, e2019JD032052, https://doi.org/ 10.1029/2019JD032052, 2020.

https://doi.org/10.5194/egusphere-2025-1463
Preprint. Discussion started: 28 May 2025

Figure captions

Fig. 1 The calculated particle losses for the Model 3321 APS spectrometer in this cruise.

Fig. 2 The total view of (a) the Model 3321 APS spectrometer and (b) the automatic meteorological observation system.

Fig. 3 The time series of the observations on 25 May 2023. The black circle represented one case of ship pollution. (a) Trends of the aerosol size distributions. (b) Trends of the rainfall intensity and the WD.

Fig. 4 The time series of the shipboard observations in the SCS from 21 May to 3 June 2023. The blue-shaded regions represented periods affected by rain events. (a) Trend of the aerosol size distributions. (b) Trends of NCs of the two aerosol particle modes (black solid line represented the NC of the coarse mode, and red solid line represented the NC of the accumulation mode). (c) Trend of the WD. (d) Trends of the T_{OBS} (dark orange solid line), T_{2m} (light orange solid line), and SST (blue solid line). (e) Trends in the RH (gray solid line), the VIS (red solid line), and the rainfall intensity (dark blue solid line).

Fig. 5 (a) NC of the aerosol accumulation mode, (b) NC of the aerosol coarse mode, (c) RH, and (d) rainfall intensity as the functions of the WS and WD for the observations in the SCS.

Fig. 6 The scatter plots of (a) NCs of the aerosol accumulation mode and WS, (b) NCs of the aerosol coarse mode and WS. The observation data were binned to the WS intervals equal to 3 m s^{-1}; the boxes represented the 25th to 75th percentile value, the black whisker represented the 1.5 inter-quartile range, the black diamond marker represented the mean value, and the black horizontal line represented the median value in the box plots.

Fig. 7 Classification of the shipboard observation path in the SCS: (a) Accumulation and coarse mode particle sizes graded NCs in the offshore and pelagic regions. For the box plots, the boxes represented the 25th to 75th percentile value, the black whisker represented the maximum and minimum range, the black triangle represented the 1.5 inter-quartile range, the black diamond marker represented the mean value, and the black horizontal line represented the median value. (b) The NCs of average size distributions (the solid lines and circles) and standard deviations (the shaded areas) for marine aerosols of 0.5 to 10 μm diameters in the offshore and pelagic regions. (c) The diurnal variations of the proportions and the NCs of two aerosol particle modes were shown with the distances from the coast. (d) The distributions of marine aerosol components in the offshore and pelagic regions. The pie charts showed the average aerosol composition based on the mass concentrations from the Merra-2 aerosol dataset during the whole cruise period.

Fig. 8 (a) The 72-h backward trajectory air mass source traces in the offshore (orange solid lines) and pelagic (blue solid lines) regions. (b) Detailed map of the backward trajectory air mass source traces passing through the mainland areas (© Google Earth).

Fig. 9 (a) Diurnal variations of the total mean values of the NCs in the different aerosol particle modes. The vertical bars showed the standard errors (the shadow areas represented the transition periods between daytime and nighttime). (b) The NCs of average size distributions for marine aerosols of 0.5 to 10 μm diameters in different time periods. (c) The NCs of the different aerosol particle modes in different time periods. For the box plots, the boxes represented the 25th to 75th percentile value, the black whisker represented the maximum and minimum range, the black triangle represented the 1.5 inter-quartile range, the black diamond marker represented the mean value, and the black horizontal line represented the median value.

Fig. 10 (a) The correlation coefficients between the NCs of all aerosol particle modes and different meteorological parameters. Correlation plot showing the Pearson correlation values of all marine aerosol NCs and meteorological parameters measured in pelagic regions. (b) The comparisons between the diurnal variations of total NCs, SST, SST-T_{2m}, and WS.

Fig. 11 The NCs versus WS in the pelagic region. The NC of all aerosol particle modes versus WS for 28-29 ℃ (a), 29-30 ℃ (b), and 30-31 ℃ (c) SST intervals. The error bars represented the standard deviations. The R represented the Pearson correlation coefficients, and the p values were performed to test whether the correlations were significant.

https://doi.org/10.5194/egusphere-2025-1463
Preprint. Discussion started: 28 May 2025

Fig. 12 The NCs versus SST in the pelagic region. The NC of all aerosol particle modes versus SST for 0-3 m s^{-1} (a), 3-6 m s^{-1} (b), 6-9 m s^{-1} (c), 9-12 m s^{-1} (d), and 12-15 m s^{-1} (e) WS intervals. The error bars represented the standard deviations. The R represented the Pearson correlation coefficients, and the p values were performed to test whether the correlations were significant.

Fig. 13 The relationship between the NC of all aerosol particle modes and WS (a), SST (b), and SST-T_{2m} (c). The error bars represented the standard deviations. The R represented the Pearson correlation coefficients, and the p values were performed to test whether the correlations were significant.

Fig. 14 The NCs versus SST-T_{2m} in the pelagic region. The NC of all aerosol particle modes versus SST-T_{2m} for 0-3 m s^{-1} (a), 3-6 m s^{-1} (b), 6-9 m s^{-1} (c), 9-12 m s^{-1} (d), and 12-15 m s^{-1} (e) WS intervals. The error bars represented the standard deviations. The R represented the Pearson correlation coefficients, and the p values were performed to test whether the correlations were significant.

Fig. 15 The NCs versus SST-T_{2m} in the pelagic region. The NC of all aerosol particle modes versus SST-T_{2m} for 28-29 ℃ (a), 29-30 ℃ (b), and 30-31 ℃ (c) SST intervals. The error bars represented the standard deviations. The R represented the Pearson correlation coefficients, and the p values were performed to test whether the correlations were significant.